

İSTANBUL TECHNICAL UNIVERSITY ★ ENERGY INSTITUTE

**ASSEMBLY HOMOGENIZATION OF LIGHT WATER REACTORS BY A
MONTE CARLO REACTOR PHYSICS METHOD AND VERIFICATION BY
A DETERMINISTIC METHOD**

**M.Sc. Thesis by
Aziz Bora PEKİÇTEN
(301081003)**

**Date of submission : 06 May 2011
Date of defence examination: 06 June 2011**

**Supervisor (Chairman) : Prof. Dr. Bilge ÖZGENER (ITU)
Members of the Examining Committee : Prof. Dr. Melih GEÇKİNLİ (ITU)
Prof. Dr. Cemal YILDIZ (ITU)**

JUNE 2011

İSTANBUL TEKNİK ÜNİVERSİTESİ ★ ENERJİ ENSTİTÜSÜ

**HAFİF SU REAKTÖRLERİNİN MONTE CARLO REAKTÖR FİZİĞİ
YÖNTEMİ İLE HOMOJENİZASYONU VE DETERMİNİSTİK YÖNTEM
İLE DOĞRULANMASI**

**YÜKSEK LİSANS TEZİ
Aziz Bora PEKİÇTEN
(301081003)**

Tezin Enstitüye Verildiği Tarih : 06 Mayıs 2011

Tezin Savunulduğu Tarih : 06 Haziran 2011

**Tez Danışmanı : Prof. Dr. Bilge ÖZGENER (İTÜ)
Diğer Jüri Üyeleri : Prof. Dr. Melih GEÇKİNLİ (İTÜ)
Prof. Dr. Cemal YILDIZ (İTÜ)**

HAZİRAN 2011

FOREWORD

I would like to express my deep appreciation and thanks for my advisors Dr. Tomasz Kozlowski and Prof. Dr. Bilge Özgener. And also I would like to thank to the Erasmus office in the European Union Centre of ITU, for giving me the chance to study abroad, and making possible this thesis work. This work is supported by Royal Institute of Technology Nuclear Power Safety Division and Istanbul Technical University Energy Institute.

May 2011

Aziz Bora Pekicten
Mechanical Engineer

TABLE OF CONTENTS

	<u>Page</u>
ABBREVIATIONS	ix
LIST OF TABLES	xi
LIST OF FIGURES	xiii
SUMMARY	xv
ÖZET	xvii
1. INTRODUCTION	1
1.1 Purpose of The Thesis	2
2. ASSEMBLY HOMOGENIZATION METHODS	3
2.1 Introduction	3
2.2 Conventional Homogenization Theory	8
2.3 Koebke’s Equivalence Theory and Smith’s General Equivalence Theory	9
3. DESCRIPTION OF TOOLS	17
3.1 Introduction	17
3.2 Serpent.....	17
3.3 PARCS	20
4. DESCRIPTION OF MINI CORE PROBLEMS	23
4.1 Main Properties of The Core Assemblies	23
4.2 Application of The Verification and The Homogenization	24
4.2.1 Generation of the assembly discontinuity factors	25
5. PRESENTATION AND DISCUSSION OF RESULTS	29
6. CONCLUSION	33
REFERENCES	35
APPENDICES	37
CURRICULUM VITA	47

ABBREVIATIONS

aADF	: Average Assembly Discontinuity Factors
ADF	: Assembly Discontinuity Factors
BWR	: Boiling Water Reactors
CANDU	: Canada Deuterium Uranium
Fig	: Figure
HTGR	: High Temperature Gas Reactors
K_{eff}	: K-effective (Effective Multiplication Factor)
LWR	: Light Water Reactors
MCNP	: Monte Carlo N-Particle
PARCS	: Purdue Advanced Reactor Core Simulator
PWR	: Pressurized Water Reactors
U.S. NRC	: United States Nuclear Regulatory Commission
U-235	: Uranium isotope-235
UDF	: Unity Discontinuity Factors
UMN	: University of Minnesota
VTT	: Technical Research Centre of Finland

LIST OF TABLES

	<u>Page</u>
Table 4.1: ADFs for fuel and reflector assemblies for combination-1.....	26
Table 4.2: Comparison of solutions of combination-1.....	26
Table 4.3: ADFs for fuel and reflector assemblies for combination-2.....	26
Table 4.4: Comparison of solutions of combination-2.....	27
Table 4.5: ADFs for fuel and reflector assemblies for combination-3.....	27
Table 4.6: Comparison of solutions of combination-3.....	27
Table 5.1: Comparison of solutions of mini core-1	29
Table 5.2: Comparison of solutions of mini core-2	29
Table 5.3: Comparison of solutions of mini core-3	29
Table 5.4: Comparison of solutions of mini core-4	29
Table 5.5: Comparison of solutions of mini core-5	30
Table 5.6: Comparison of solutions of mini core-6	30
Table 5.7: Comparison of solutions of mini core-7	30
Table 5.8: Comparison of solutions of mini core-8	30
Table 5.9: Comparison of solutions of mini core-9	30
Table 5.10: Comparison of solutions of mini core-10	30
Table 5.11: Comparison of solutions of mini core-11	31
Table 5.12: Comparison of solutions of mini core-12	31
Table 5.13: Comparison of solutions of mini core-13	31
Table 5.14: Comparison of solutions of mini core-14	31

LIST OF FIGURES

	<u>Page</u>
Figure 2.1 : A cell with fuel and moderator elements.....	3
Figure 2.2 : Wigner-Seitz approximation.	5
Figure 2.3 : Representation of the Newmarch effect.	5
Figure 2.4 : Assembly homogenization.	9
Figure 2.5 : Reactor core consisting of homogenized assemblies.	10
Figure 2.6 : Assembly (i,j).	11
Figure 4.1 : The cross section area of the fuel pin.	23
Figure 4.2 : Geometry of combination-1.	25
Figure 4.3 : Geometry of combination-2.	25
Figure 4.4 : Geometry of combination-3.	26
Figure A.1 : Surface plots of errors of designing ADFs for combination-1	38
Figure A.2 : Surface plots of errors of designing ADFs for combination-2	39
Figure A.3 : Surface plots of errors of designing ADFs for combination-3	41
Figure B.1 : Configuration of the geometry for each core.....	43

ASSEMBLY HOMOGENIZATION OF LIGHT WATER REACTORS BY A MONTE CARLO REACTOR PHYSICS METHOD AND VERIFICATION BY A DETERMINISTIC METHOD

SUMMARY

Assembly homogenization is an important part of reactor core physics analysis. The loading of fuel assemblies in a commercial nuclear power plant is an important step before the startup of the reactor. The physical reactor core is modeled in computer environment. Distribution of fissile materials is decided after reactor physics code calculations. Many different reactor physics codes are used with calculations taking weeks or months. The purpose in this study is to test and verify the assembly homogenization capability of a Monte-Carlo reactor physics code called Serpent, which is used for the last years and is being used widely each year, and is faster than the previous ones.

In this study, Serpent did assembly homogenization of several different core configurations in two-dimensional geometry, and the results were tested in deterministic reactor simulation code called PARCS. Results showed that Serpent is capable to generate few-group constants for LWR-type assemblies. However, the assembly discontinuity factors generation by Serpent for fuel-reflector interface was not correct, so the objective of this thesis was to generate appropriate fuel-reflector discontinuity factors by off-line calculation, without access to the reference interface current. With the appropriately generated discontinuity factors, the results showed that assembly homogenization by Serpent is accurate to less than 0.5% k_{eff} error and less than 1.0% assembly flux ratio (the ratio of the averaged fast group of flux to the averaged thermal group of flux in the assembly).

HAFIF SU REAKTÖRLERİNİN MONTE CARLO REAKTÖR FİZİĞİ YÖNTEMİ İLE HOMOJENİZASYONU VE DETERMİNİSTİK YÖNTEM İLE DOĞRULANMASI

ÖZET

Reaktör demet homojenizasyonu reaktör kalbi fiziksel analizlerinin önemli bir bölümüdür. Yakıt elemanlarının yüklenmesi, günümüz nükleer santrallerinde reaktörün çalışmasının başlangıcı öncesi için önemli bir adımdır. Fiziksel reaktör kalbi bilgisayar ortamında modellenir. Fisil maddelerin dağılımlarının kararı reaktör fiziği kodu hesaplamalarından sonra verilir. Hesaplamaları haftalar ve aylar süren bir çok farklı reaktör fiziği kodları vardır ve kullanılır. Bu çalışmanın amacı, son bir kaç yıldır kullanılan ve geçen her sene boyunca yaygınlaşan, öncekilere göre daha hızlı hesaplamalar yapabilen, Serpent adındaki Monte-Carlo reaktör fiziği kodunun homojenizasyon kabiliyetini test etmek ve doğrulamaktır.

Bu çalışmada değişik şekilde düzenlenmiş reaktör kalbi konfigürasyonlarının demet homojenizasyonu iki-boyutlu geometride Serpent kodu tarafından yapılmış ve sonuçlar deterministik reaktör simulasyon kodu olan PARCS ile kontrol edilmiştir. Sonuçlar Serpent kodunun hafif su reaktör tipi demetler için grup kesit alanı üretiminin uygun olduğunu gösterdi. Ama yakıt-reflektör arayüzü için demet devamsızlık faktörleri üretimi doğru değildi. Bu yüzden bu tezin amacı, referans arayüz akı verilerine sahip olmadan, kapalı bir yöntemle yakıt-reflektör arayüzü için doğru devamsızlık faktörleri üretimidir. Üretilen doğru devamsızlık faktörleri ile sonuçlar, Serpent kodu tarafından gerçekleştirilen demet homojenizasyonunun çok küçük hata yüzdesi ile yanlışsız olduğu görülmüştür. Hata yüzdeleri keff için 0.5%'in altında ve akı oranları (demet içindeki ortalama hızlı grup akısının ortalama termal grup akısına oranı) için 1.0%'in altında olduğu görülmüştür.

1. INTRODUCTION

Extensive knowledge of different quantities is necessary for the physics design and analysis of light water reactors. The prediction of neutron density in space, direction and energy increases the ability to perform core-follow calculations where the determination of power distribution, control rod worth, shutdown margins and isotopic depletion rates must be known. With the assumption that thermal-hydraulic properties of the reactor and fundamental data are known, three-dimensional neutron transport equation is a task need to be solved. Explicit modeling of water channels, fuel pins, control rods and burnable poisons limits the direct methods of solving the three-dimensional transport equation. Tools such as three-dimensional continuous energy Monte Carlo and deterministic neutron transport methods are similarly overwhelmed by the complexity of the computational problem of explicit geometrical modeling on a core-wide basis.

Many reactor analysis methods circumvent the computational burden of explicit geometrical modeling by coupling geometrically-simple, energy-intensive calculations with few-group, geometrically-complicated calculations via spatial homogenization and group condensation. The question how to make the best use of spatial and spectral distributions of reaction rates and neutron densities has prompted several different approaches to reactor analysis.

Alternative methods, which can all be put in a general class called nodal diffusion methods have been developed over the years. These nodal methods have been capable of solving three-dimensional neutron diffusion equation with a less than 2% error in assemble-averaged powers using assembly-size mesh. The assumption of these nodal methods is that to obtain “equivalent” diffusion theory parameters, which are spatially constant over the whole cross sectional area of a fuel assembly, pin-by-pin lattice cross sections have been spatially homogenized. The nodal solution provides only nodal (volume-averaged) and surface (face-averaged) fluxes and reaction rates. It is important that accurate methods for homogenizing reactor assemblies are developed and employed.

1.1 Purpose of The Thesis

The major aim of this thesis is to perform assembly homogenization in two-dimensional LWR mini-cores with possible fuel and reflector assembly configurations. Homogenization techniques will be applied using Serpent (Monte Carlo reactor physics code) and verified by PARCS (deterministic reactor simulation code).

2. ASSEMBLY HOMOGENIZATION METHODS

2.1 Introduction

A number of homogenization techniques determine diffusion coefficients by matching certain components of heterogeneous model properties. Consider a symmetric, repeating array of fuel and moderator elements of volume V_F and V_M . One unit in the array is a cell (see Fig. 2.1).

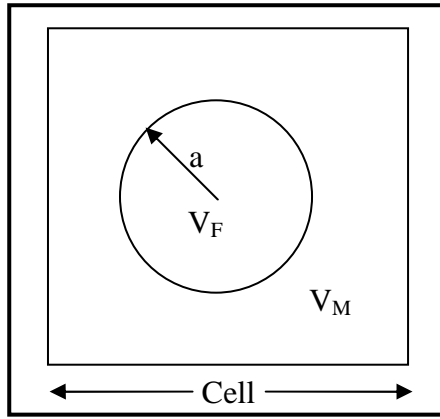


Figure 2.1 : A cell with fuel and moderator elements.

The absorption rate in the cell, A^{hetero} ;

$$A^{hetero} = \Sigma_a^F \phi_F V_F + \Sigma_a^M \phi_M V_M \quad (2.1)$$

where Σ_a^F, Σ_a^M are the absorption cross sections; ϕ_F, ϕ_M are volume averaged fluxes.

We want to design a homogeneous system where the moderator and fuel are mixed. We also want the average flux in the homogeneous system to be equal to that of the real cell. We want to determine a $\langle \Sigma_a \rangle_{cell}$ for this homogeneous system so that its absorption rate equals that of the heterogeneous cell.

$$A^{homo} = \langle \Sigma_a \rangle_{cell} \phi_{cell} V_{cell} \quad (2.2)$$

$$\text{where } \phi_{cell} = \frac{\phi_F V_F + \phi_M V_M}{V_{cell}}$$

$$\text{or } A^{homo} = \langle \Sigma_a \rangle_{cell} (\phi_F V_F + \phi_M V_M).$$

If A^{hetero} equals to A^{homo} , then;

$$\langle \Sigma_a \rangle_{\text{cell}} = \frac{\Sigma_a^F \phi_F V_F + \Sigma_a^M \phi_M V_M}{\phi_F V_F + \phi_M V_M} \quad (2.3)$$

Dividing the numerator and denominator by $\phi_F V_F$;

$$\langle \Sigma_a \rangle_{\text{cell}} = \frac{\Sigma_a^F + \Sigma_a^M (V_M/V_F) \xi}{1 + (V_M/V_F) \xi} \quad (2.4)$$

where $\xi = \frac{\phi_M}{\phi_F}$ and is flux disadvantage factor. This methodology does not apply directly to the diffusion coefficient “D” since it is related to leakage. For multiregional cells ($I > 2$);

$$\langle \Sigma_x \rangle_{\text{cell}} = \frac{\Sigma_x^1 + \sum_{i=2}^I \Sigma_x^i (V_i/V_1) \xi_i}{1 + \sum_{i=2}^I (V_i/V_1) \xi_i} \quad (2.5)$$

$$\text{and } \xi_i = \frac{\phi_i}{\phi_1}, \phi_{\text{cell}} = \frac{\sum_{i=1}^I \phi_i V_i}{V_{\text{cell}}}.$$

A fuel assembly consists of a large number of pins, which might have differing composition, each of which is clad and surrounded by moderator. A unit cell or pin cell consist of a fuel pin, cladding and surrounding moderator. The first step in homogenizing the fuel assembly is to homogenize each of the pin cells by calculating the multigroup flux distribution in the fuel cell and using it to calculate homogenized cross sections for the pin cell.

Although the calculation of the homogenized pin cell cross sections could be made by combining an infinite medium calculation with some method for estimating the disadvantage factor, today more advanced methods based on transport theory are preferred.

A simplifying assumption is that the pin cell could be considered part of an infinite array identical pin cells and thus reflective boundary conditions at cell boundary are used to model such an infinite system. But existence of the fuel pin of differing enrichment, control pins, burnable poisons etc. makes such an approach questionable. The influence of the surroundings is usually introduced by specifying a partial inward current J and an albedo β .

Since the fuel pin cells are cylindrical, it is convenient to approximate the actual pin cell geometry by an equivalent cylindrical cell that preserves moderator volume. The equivalent cylindrical cell is called Wigner-Seitz cell (see Fig. 2.2).

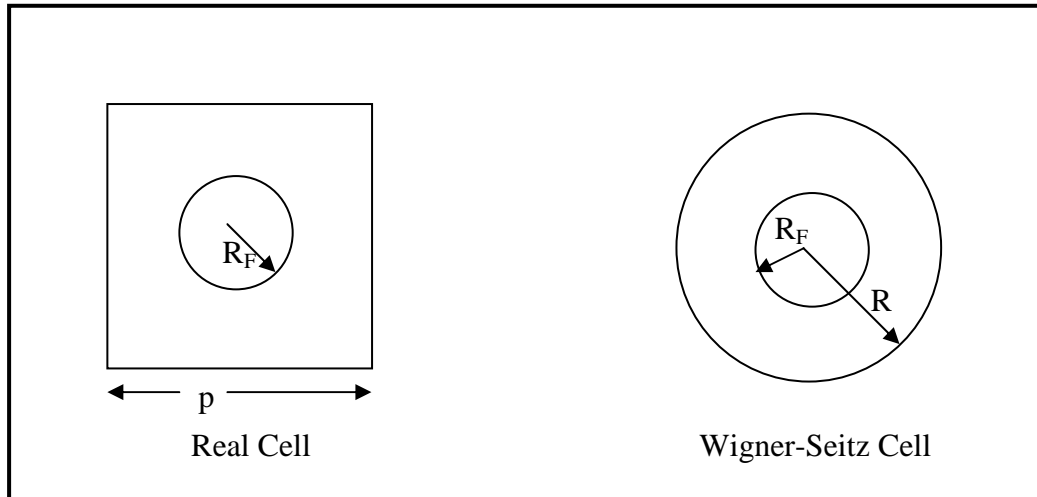


Figure 2.2 : Wigner-Seitz approximation.

Wigner-Seitz approximation converts a two-dimensional problem to a one-dimensional problem and is extensively used. However, the change from the real geometry to cylindrical geometry leads to an anomalously high flux in the moderator of the Wigner-Seitz cell when reflective boundary conditions are used. This effect is called Newmarch effect (see Fig. 2.3).

Newmarch effect arises because a neutron, introduced into the cell traveling in the direction of chord that does not pass through the fuel pin before intersection the reflecting cell boundary, will never pass through the fuel pin since reflection from the cylindrical surface will result in motion along a similar chord. On the other hand, reflection in the real cell will cause motion into the fuel pin.

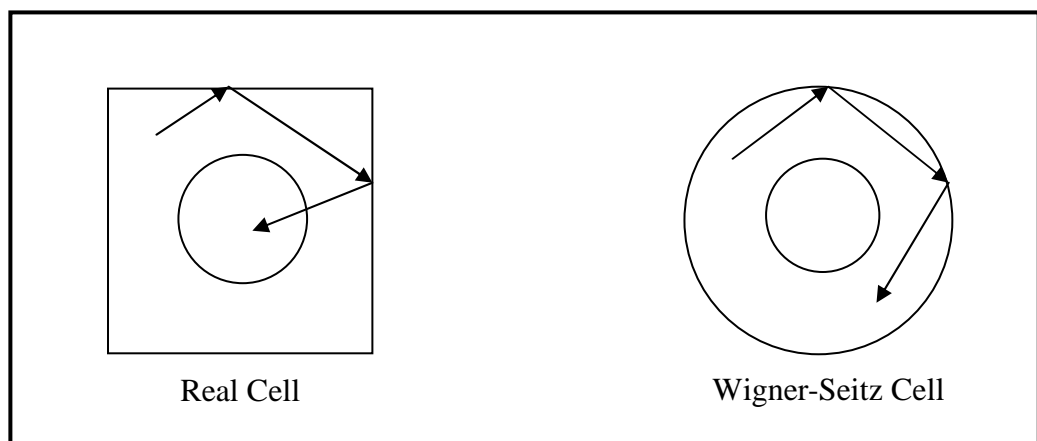


Figure 2.3 : Representation of the Newmarch effect.

Newmarch effect could be remedied by employing white boundary condition at the cylindrical boundary. The white boundary condition assumes that a neutron that hits the boundary will be returned with a cosine distribution, i.e. as if the returning neutron comes from an infinite outside region with uniform isotopic sources. The Wigner-Seitz approximation, combined with white reflection, gives excellent results and is therefore well established in pin cell calculations.

If the pin cell-to-pin cell leakage is to be taken into account, the concept of albedo, or reflection coefficient, is also employed. The albedo β ,

$$\beta = \frac{J_s^-}{J_s^+} \quad (2.6)$$

where “s” represents the cylindrical outer surface of the Wigner-Seitz cell.

Pin cell calculation are usually carried out using the collision probability method based on integral transport equation since it involves scalar flux instead of angular flux. But its basic drawback is the isotropic scattering assumption. To take linearly anisotropic scattering at least approximately into account, there is a prescription, called transport correction which is usually employed in collision probability applications. Transport correction which involves the subtraction of the quantity $\mu_0 \Sigma_{s,g}$. Transport corrected group cross sections are:

$$\Sigma_{s,g}^{tr} = \Sigma_{s,g} - \bar{\mu}_{0,g} \Sigma_{s,g} \quad (2.7)$$

$$\Sigma_{t,g}^{tr} = \Sigma_{t,g} - \bar{\mu}_{0,g} \Sigma_{s,g} \quad (2.8)$$

$$\Sigma_{s,g \rightarrow g}^{tr} = \Sigma_{s,g \rightarrow g} - \bar{\mu}_{0,g} \Sigma_{s,g} \quad (2.9)$$

Usually the transport correction and the superscript “tr” is universally omitted. Once pin cell homogenization is completed, the assembly is made up of a large number of homogeneous regions (e.g. the homogenized, usually square, pin cells) surrounded by structure, water gaps, control rods, etc.

The next step in the homogenization process is to perform a multigroup transport calculation on the pin cell homogenized assembly for the purpose of obtaining average group fluxes for each homogenized pin cell that can be used to calculate homogenized cross sections that will allow the entire assembly to be represented as a single homogenized region.

Any of the transport method or even diffusion theory in some cases can be used for the full assembly transport calculation. Such calculations are normally performed using reflective condition on the assembly boundary.

Heterogeneous system is described by multigroup transport theory as in (2.10).

$$\vec{\nabla} \cdot \vec{J}_g(\vec{r}) + \Sigma_t^g(\vec{r})\phi_g(\vec{r}) = \sum_{g'=1}^G \Sigma_{g' \rightarrow g} \phi_{g'}(\vec{r}) + \frac{\chi^g}{k} \sum_{g'=1}^G \nu \Sigma_{f,i}^{g'} \phi_{g'}(\vec{r}) \quad (2.10)$$

We imagine that we know the solution to (2.10) and wish to use it to define homogenized cross sections. We divide heterogeneous system into N homogenization regions. We wish to define homogenized cross sections $\hat{\Sigma}_{t,i}^g, \hat{\Sigma}_i^{g' \rightarrow g}, \nu \hat{\Sigma}_{f,i}^g$ so that the homogenized transport equation:

$$\vec{\nabla} \cdot \hat{J}_g(\vec{r}) + \hat{\Sigma}_{t,i}^g \hat{\phi}_g(\vec{r}) = \sum_{g'=1}^G \hat{\Sigma}_i^{g' \rightarrow g} \hat{\phi}_{g'}(\vec{r}) + \frac{\chi^g}{\hat{k}} \sum_{g'=1}^G \nu \hat{\Sigma}_{f,i}^{g'} \hat{\phi}_{g'}(\vec{r}) \quad (2.11)$$

is obeyed for $i=1,2,\dots,N$. Denoting the volume of the i 'th homogenized region by V_i and its k 'th surface by S_i^k , we require:

$$\hat{\Sigma}_{x,i}^g \int_{V_i} \hat{\phi}_g(\vec{r}) dV = \int_{V_i} \Sigma_x^g(\vec{r}) \phi_g(\vec{r}) dV \quad \begin{array}{l} x = a, t, f, s, \dots \\ i = 1, 2, \dots, N \end{array} \quad (2.12)$$

and

$$\int_{S_i^k} \vec{n} \cdot \hat{J}_g(\vec{r}) dS = \int_{S_i^k} \vec{n} \cdot \vec{J}_g(\vec{r}) dS \quad \begin{array}{l} i = 1, 2, \dots, N \\ k = 1, 2, \dots, K(i) \end{array} \quad (2.13)$$

where $K(i)$ is the number of surfaces of the i 'th homogenization region. If (2.12) and (2.13) are satisfied, obviously:

$$k = \hat{k} \quad (2.14)$$

Thus, homogenizes cross sections are defined by:

$$\hat{\Sigma}_{x,i}^g = \frac{\int_{V_i} \Sigma_x^g(\vec{r}) \phi_g(\vec{r}) dV}{\int_{V_i} \hat{\phi}_g(\vec{r}) dV} \quad (2.15)$$

and when diffusion theory is to be used in the homogenized calculation:

$$\hat{D}_{ik}^g = \frac{- \int_{S_i^k} \vec{n} \cdot \vec{J}_g(\vec{r}) dS}{\int_{S_i^k} \vec{n} \cdot \vec{\nabla} \hat{\phi}_g(\vec{r}) dS} \quad (2.16)$$

Even if we know the exact solution of (2.10) we would be knowing only the numerators of (2.15) and (2.16). To find the denominator, we need to solve homogenized transport equation (2.11). Since homogenized cross sections are needed for the solution of the homogenized diffusion equation, there seems to be a vicious circle. Nevertheless, by an iterative process, the homogenized cross sections (2.15) and (2.16) could be determined. That is, at least philosophically, homogenization seems possible.

(2.16) shows that the homogenized diffusion coefficients would take different values on different surfaces of a homogenization region. Thus, it is not possible to define a unique \hat{D}_i^g for each homogenization region.

2.2 Conventional Homogenization Theory

In conventional pin cell or assembly homogenization procedure, the solution of the heterogeneous system, $\phi_g(\vec{r})$ and $J^g(\vec{r})$ are approximated by $\phi_A^g(\vec{r})$ and $J_A^g(\vec{r})$ which are approximate solutions to the heterogeneous system at the pin cell or assembly level. $\phi_A^g(\vec{r})$ and $J_A^g(\vec{r})$ are usually obtained with zero current boundary conditions. Both in the numerator and the denominator of (2.15), $\phi_A^g(\vec{r})$ are used.

$$\hat{\Sigma}_{x,i}^g \equiv \frac{\int_{V_i} \Sigma_x^g(\vec{r}) \phi_A^g(\vec{r}) dV}{\int_{V_i} \phi_A^g(\vec{r}) dV} \quad (2.17)$$

A possible choice for the homogenized diffusion coefficient is:

$$\hat{D}_i^g \equiv \frac{\int_{V_i} D^g(\vec{r}) \phi_A^g(\vec{r}) dV}{\int_{V_i} \phi_A^g(\vec{r}) dV} \quad (2.18)$$

Rather large errors have been found in calculations that employed such conventional homogenization methods when compared with exact solution. The major source of errors is in the treatment of the diffusion coefficients.

The continuity of flux and current at interfaces between homogenization regions seems also a source of problem. The homogenized diffusion equation, with continuity of current and flux at interfaces, lacks sufficient degree of freedom to preserve both reaction rates and surface currents. [1]

2.3 Koebke's Equivalence Theory and Smith's General Equivalence Theory

Equivalence theory involves assembly homogenization. Homogenization at the pin cell level (see Fig. 2.4) is completed, and homogenized pin cell group cross sections are assumed to be available:

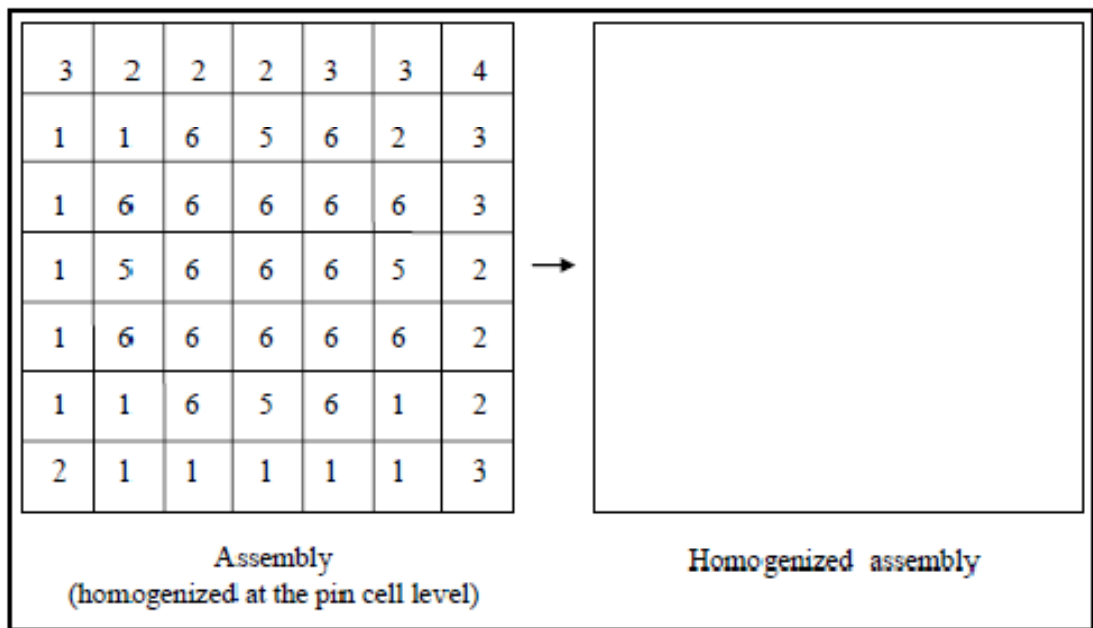


Figure 2.4 : Assembly homogenization.

Since whole core calculations are usually carried out, after assembly homogenization, by nodal methods, assembly homogenization involves variables which are defined in the nodal method terminology. Equivalence homogenization is closely associated with transverse integrated nodal methods. We assume a two dimensional model of the assembly and assume the existence of an exact transport solution for the assembly homogenized at the pin cell level. [2]

$$\vec{\nabla} \cdot \vec{J}_g(\vec{r}) + \Sigma_t^g(\vec{r})\phi_g(\vec{r}) = \sum_{g'=1}^G \Sigma^{g' \rightarrow g}(\vec{r})\phi_{g'}(\vec{r}) + \frac{\chi^g}{k} \sum_{g'=1}^G \nu \Sigma_f^{g'}(\vec{r})\phi_{g'}(\vec{r}) \quad (2.19)$$

The equivalent homogenized assembly is a part of the reactor core and consists of other homogenized assemblies. Each assembly is denoted by (i, j) where “i” denotes the row number and “j” the column number (see Fig. 2.5).

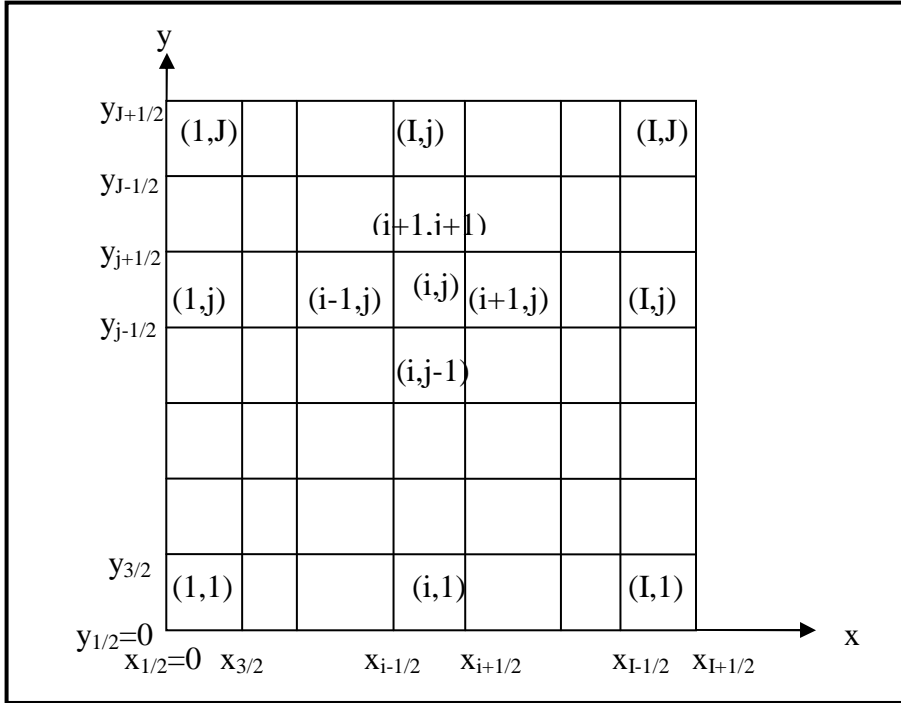


Figure 2.5 : Reactor core consisting of homogenized assemblies.

We denote the cross sections of the homogenized assembly (i, j) by $\hat{\Sigma}_{x,i,j}$ and the flux and the current by $\hat{\phi}$ and \hat{J} respectively. The homogenized transport equation for assembly (i, j) is:

$$\vec{\nabla} \cdot \hat{J}_g(\vec{r}) + \hat{\Sigma}_{i,i,j}^g \phi_g(\vec{r}) = \sum_{g'=1}^G \hat{\Sigma}_{i,i,j}^{g' \rightarrow g} \hat{\phi}_{g'}(\vec{r}) + \frac{\chi^g}{k} \sum_{g'=1}^G \nu \hat{\Sigma}_{f,i,j}^{g'} \hat{\phi}_{g'}(\vec{r}), \quad \vec{r} \in V^{(i,j)} \quad (2.20)$$

To inquire whether homogenization is theoretically possible, we assume that we know the exact transport solution $\phi_g(\vec{r})$ and $\vec{J}_g(\vec{r})$ and try to determine the homogenized constants $\hat{\Sigma}_{x,i,j}$ which would give reaction and leakage rates for the homogenized assembly which are identical to their counterparts in the nonhomogenized assembly.

We consider the assembly (i, j) (see Fig. 2.6):

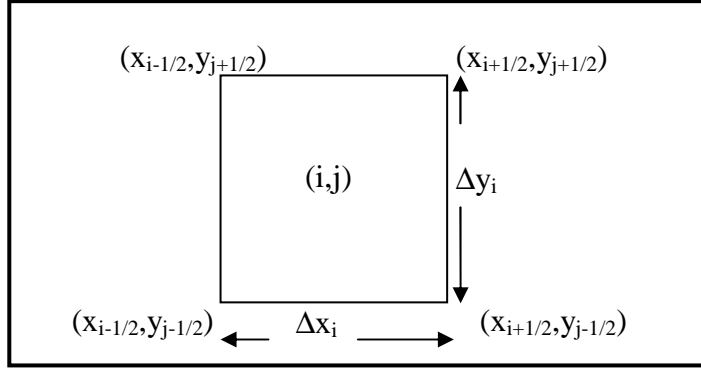


Figure 2.6 : Assembly (i, j).

We integrate (2.19) over the assembly (i, j) to obtain:

$$\begin{aligned} \Delta y_j \left(J_{i+1/2, j}^{g^-} - J_{i-1/2, j}^{g^+} \right) + \Delta x_i \left(J_{i, j+1/2}^{g^-} - J_{i, j-1/2}^{g^+} \right) + \Sigma_{t, i, j}^g \phi_{i, j}^g \Delta x_i \Delta y_j = \\ \sum_{g'=1}^G \Sigma_{i, j}^{g' \rightarrow g} \phi_{i, j}^{g'} \Delta x_i \Delta y_j + \frac{\chi^g}{k} \sum_{g'=1}^G v \Sigma_{f, i, j}^{g'} \phi_{i, j}^{g'} \Delta x_i \Delta y_j \end{aligned} \quad (2.21)$$

where:

$$\phi_{i, j}^g = \frac{1}{\Delta x_i \Delta y_j} \int_{x_{i-1/2}}^{x_{i+1/2}} \int_{y_{j-1/2}}^{y_{j+1/2}} \phi_g(x, y) dx dy \quad (2.22)$$

$$\Sigma_{x, i, j}^g = \frac{1}{\phi_{i, j}^g \Delta x_i \Delta y_i} \int_{x_{i-1/2}}^{x_{i+1/2}} \int_{y_{j-1/2}}^{y_{j+1/2}} \Sigma_x^g(x, y) \phi_g(x, y) dx dy \quad (2.23)$$

The edge averaged currents are defined as:

$$J_{i\pm 1/2, j}^{g^\mp} = \frac{1}{\Delta y_j} \int_{y_{j-1/2}}^{y_{j+1/2}} \vec{n}_x \cdot \vec{J}^g(x_{i\pm 1/2}, y) dy \quad (2.24)$$

$$J_{i, j\pm 1/2}^{g^\mp} = \frac{1}{\Delta x_i} \int_{x_{i-1/2}}^{x_{i+1/2}} \vec{n}_y \cdot \vec{J}^g(x, y_{j\pm 1/2}) dx \quad (2.25)$$

The (-) and (+) superscripts are used to denote location of the assembly (i, j) with respect to the edge. If we integrate the homogenized equation similarly, we obtain:

$$\begin{aligned} \Delta y_j \left(\hat{J}_{i+1/2, j}^{g^-} - \hat{J}_{i-1/2, j}^{g^+} \right) + \Delta x_i \left(\hat{J}_{i, j+1/2}^{g^-} - \hat{J}_{i, j-1/2}^{g^+} \right) + \hat{\Sigma}_{t, i, j}^g \hat{\phi}_{i, j}^g \Delta x_i \Delta y_j = \\ \sum_{g'=1}^G \hat{\Sigma}_{i, j}^{g' \rightarrow g} \hat{\phi}_{i, j}^{g'} \Delta x_i \Delta y_j + \frac{\chi^g}{k} \sum_{g'=1}^G v \hat{\Sigma}_{f, i, j}^{g'} \hat{\phi}_{i, j}^{g'} \Delta x_i \Delta y_j \end{aligned} \quad (2.26)$$

where:

$$\hat{J}_{i\pm 1/2,j}^{g\mp} = \frac{1}{\Delta y_j} \int_{y_{j-1/2}}^{y_{j+1/2}} \vec{n}_x \cdot \hat{J}^g(x_{i\pm 1/2}^{\mp}, y) dy \quad (2.27)$$

$$\hat{J}_{i,j\pm 1/2}^{g\mp} = \frac{1}{\Delta x_i} \int_{x_{i-1/2}}^{x_{i+1/2}} \vec{n}_y \cdot \hat{J}^g(x, y_{j\pm 1/2}^{\mp}) dx \quad (2.28)$$

$$\hat{\phi}_{i,j}^g = \frac{1}{\Delta x_i \Delta y_j} \int_{x_{i-1/2}}^{x_{i+1/2}} \int_{y_{j-1/2}}^{y_{j+1/2}} \hat{\phi}_g(x, y) dx dy \quad (2.29)$$

Since we assume that we knew the heterogeneous exact solution, we choose the homogenized constants such that:

$$\hat{\Sigma}_{x,i,j}^g = \Sigma_{x,i,j}^g \quad (2.30)$$

If the quality of the edge currents in (2.21) and (2.26) can also be enforced, the cell averaged fluxes of (2.21) and (2.26) would be equal:

$$\hat{\phi}_{i,j}^g = \phi_{i,j}^g \quad (2.31)$$

Thus both the reaction rates and the leakage through the edges would be identical to the exact solution.

We have shown that an assembly homogenization, which preserves both reaction rates and leakage, is possible if we knew the exact solution for the heterogeneous assembly, which is possibly homogenized at the pin cell level. Moreover, the homogenized diffusion coefficient seems to be arbitrary and has not been a factor in our considerations.

The homogenized edge fluxes, are defined as:

$$\hat{\phi}_{i\pm 1/2,j}^{g\mp} = \frac{1}{\Delta y_j} \int_{y_{j-1/2}}^{y_{j+1/2}} \phi^g(x_{i\pm 1/2}^{\mp}, y) dy \quad (2.32)$$

$$\hat{\phi}_{i,j\pm 1/2}^{g\mp} = \frac{1}{\Delta x_i} \int_{x_{i-1/2}}^{x_{i+1/2}} \phi^g(x, y_{j\pm 1/2}^{\mp}) dx$$

would be discontinuous.

That is:

$$\begin{aligned}\hat{\phi}_{i+1/2,j}^{g^-} &\neq \hat{\phi}_{i+1/2,j}^{g^+} \\ \hat{\phi}_{i,j+1/2}^{g^-} &\neq \hat{\phi}_{i,j+1/2}^{g^+}\end{aligned}\tag{2.33}$$

On the other hand, the exact fluxes:

$$\begin{aligned}\phi_{i\pm 1/2,j}^{g^\mp} &= \frac{1}{\Delta y_j} \int_{y_{j-1/2}}^{y_{j+1/2}} \phi^g(x_{i\pm 1/2}, y) dy \\ \phi_{i,j\pm 1/2}^{g^\mp} &= \frac{1}{\Delta x_i} \int_{x_{i-1/2}}^{x_{i+1/2}} \phi^g(x, y_{i,j\pm 1/2}) dx\end{aligned}\tag{2.34}$$

are certainly continuous. That is:

$$\begin{aligned}\phi_{i+1/2,j}^{g^-} &= \phi_{i+1/2,j}^{g^+} \\ \phi_{i,j+1/2}^{g^-} &= \phi_{i,j+1/2}^{g^+}\end{aligned}\tag{2.35}$$

At this point we define discontinuity factors:

$$\begin{aligned}f_{i,j}^{g(x)^-} &= \frac{\phi_{i+1/2,j}^{g^-}}{\hat{\phi}_{i+1/2,j}^{g^-}}, & f_{i,j}^{g(x)^+} &= \frac{\phi_{i-1/2,j}^{g^+}}{\hat{\phi}_{i-1/2,j}^{g^+}} \\ f_{i,j}^{g(y)^-} &= \frac{\phi_{i,j+1/2}^{g^-}}{\hat{\phi}_{i,j+1/2}^{g^-}}, & f_{i,j}^{g(y)^+} &= \frac{\phi_{i,j-1/2}^{g^+}}{\hat{\phi}_{i,j-1/2}^{g^+}}\end{aligned}\tag{2.36}$$

The imposition of (2.35) requires:

$$\begin{aligned}f_{i,j}^{g(x)^-} \hat{\phi}_{i+1/2,j}^{g^-} &= f_{i+1,j}^{g(x)^+} \hat{\phi}_{i+1/2,j}^{g^+} \\ f_{i,j}^{g(x)^+} \hat{\phi}_{i-1/2,j}^{g^+} &= f_{i-1,j}^{g(x)^-} \hat{\phi}_{i-1/2,j}^{g^-} \\ f_{i,j}^{g(y)^-} \hat{\phi}_{i,j+1/2}^{g^-} &= f_{i,j+1}^{g(y)^+} \hat{\phi}_{i,j+1/2}^{g^+} \\ f_{i,j}^{g(y)^+} \hat{\phi}_{i,j-1/2}^{g^+} &= f_{i,j-1}^{g(y)^-} \hat{\phi}_{i,j-1/2}^{g^-}\end{aligned}\tag{2.37}$$

Thus, during whole core calculations, the homogeneous flux becomes discontinuous, to preserve the continuity of the heterogeneous flux as in (2.35). However, everything we have done so far has only theoretical value since the exact solution of (2.19) will not be known. So we need an approximate solution to heterogeneous problem (2.19). So we define the approximate solution $\phi_A^g(\vec{r})$ as the solution of:

$$\vec{\nabla} \cdot \vec{J}_A^g(\vec{r}) + \Sigma_t^g(\vec{r}) \phi_A^g(\vec{r}) = \sum_{g'=1}^G \Sigma_{g' \rightarrow g}^g(\vec{r}) \phi_A^{g'}(\vec{r}) + \frac{\mathcal{X}^g}{k} \sum_{g'=1}^G \nu \Sigma_f^{g'}(\vec{r}) \phi_A^{g'}(\vec{r})\tag{2.38}$$

with zero current boundary condition:

$$\vec{n} \cdot \vec{\nabla} \phi_A^g(\vec{r}) = 0, \quad \vec{r} \in S \quad (2.39)$$

“S” is the union of the four sides of the assembly. Using approximate heterogeneous solution $\phi_A^g(\vec{r})$ in (2.22), (2.23) and (2.29):

$$\hat{\Sigma}_{x,i,j}^g = \frac{\int_{x_{i-1/2}}^{x_{i+1/2}} \int_{y_{j-1/2}}^{y_{j+1/2}} \Sigma_x^g(x, y) \phi_A^g(x, y) dy}{\int_{x_{i-1/2}}^{x_{i+1/2}} \int_{y_{j-1/2}}^{y_{j+1/2}} \phi_A^g(x, y) dy} \quad (2.40)$$

But (2.40) is no different than the result of the conventional homogenization theory. So the homogenized cross sections have the same definition in the conventional and equivalence homogenization theories. Diffusion coefficient is not needed for establishing continuity of current across assemblies in equivalence theory. But since it is still needed in whole core calculations, (2.40) could be employed to calculate

$$\hat{\Sigma}_{tr,i,j}^g. \text{ Then } D_{i,j}^g = \frac{1}{3\hat{\Sigma}_{tr,i,j}^g} \text{ would give us the diffusion coefficient.}$$

The only difference between the conventional and equivalence homogenization theories is in the continuity of flux across assembly boundaries. Whereas conventional theory assumes continuity, equivalence homogenization theory requires discontinuity in homogenized solution as in (2.37). thus we need to evaluate the flux discontinuity factors of (2.36) to apply equivalence homogenization theory. Since the numerators in (2.36) involve $\phi_{i+1/2,j}^g$ etc., which we do not know, we approximate with $\phi_{A,i+1/2,j}^g$. The denominators in (2.36) have to be the homogeneous counterpart of the heterogeneous approximate solution $\phi_A^g(\vec{r})$. We call it $\hat{\phi}_A^g(\vec{r})$.

Since $\phi_A^g(\vec{r})$ involves zero-current boundary condition at assembly boundary, $\hat{\phi}_A^g(\vec{r})$ is subject to the same boundary conditions. Since $\hat{\phi}_A^g(\vec{r})$ is the solution of a homogenized system (spatially constant cross section), and zero-current boundary condition makes it a part of an infinite system, $\hat{\phi}_A^g(\vec{r})$ is constant. That is:

$$\hat{\phi}_{A,i+1/2,j}^{g-} = \hat{\phi}_{A,i-1/2,j}^{g+} = \hat{\phi}_{A,i,j+1/2}^{g-} = \hat{\phi}_{A,i,j-1/2}^{g+} = \hat{\phi}_{A,i,j}^g \quad (2.41)$$

But by (2.30):

$$\hat{\phi}_{A,i,j}^g = \phi_{A,i,j}^g \quad (2.42)$$

Thus:

$$\begin{aligned} f_{i,j}^{g(x)^-} &= \frac{\phi_{A,i+1/2,j}^g}{\phi_{A,i,j}^g}, & f_{i,j}^{g(x)^+} &= \frac{\phi_{A,i-1/2,j}^g}{\phi_{A,i,j}^g} \\ f_{i,j}^{g(y)^-} &= \frac{\phi_{A,i,j+1/2}^g}{\phi_{A,i,j}^g}, & f_{i,j}^{g(y)^+} &= \frac{\phi_{A,i,j-1/2}^g}{\phi_{A,i,j}^g} \end{aligned} \quad (2.43)$$

That is discontinuity factor for any edge is simply the ratio of the edge average flux to the assembly average flux. The flux discontinuity factors are also called assembly discontinuity factors. Equivalence theory is accurate especially for assemblies for which there is no significant inter-assembly leakage. Formulation of equivalence theory is appropriate for any nodal method that uses edge-average fluxes. [3]

3. DESCRIPTION OF TOOLS

3.1 Introduction

The purpose of this study is to verify the results for a defined core configuration created by a Monte Carlo reactor physics code with a deterministic reactor physics code. The Monte Carlo reactor physics code used in this thesis work is called Serpent, which is a code developed by VTT. The deterministic code is three-dimensional reactor simulator code called PARCS developed by Purdue University and U.S. NRC.

3.2 Serpent

Serpent is a three-dimensional Monte Carlo reactor physics code developed at VTT since 2004. The code is specialized in two-dimensional lattice physics calculations but it is possible to model complicated three-dimensional geometries also. The code is capable of generating homogenized multi-group constants for deterministic reactor core simulators, burn-up calculations for fuel cycle studies and research reactors, demonstration of reactor physics phenomena and for educational studies.

Serpent uses a universe-based geometry where it is easy to describe two or three-dimensional designs. Material cells and surface types are the basis of the geometry. There are many features to describe cylindrical fuel pins and spherical fuel particles, square and hexagonal lattices, circular cluster arrays for CANDU fuels, and fuel definition for HTGR cores.

Combination of conventional surface-to-surface ray-tracing and the Woodcock delta-tracking method have an efficient geometry routine for lattice calculations. The track-length estimate of neutron flux in delta-tracking is not efficient for small or thin volumes located far from active source.

Serpent reads cross sections from ACE format libraries where classical collision kinematics and ENDF reaction laws are the basis of the interaction physics. The data in libraries is available for 432 nuclides at temperatures of 300, 600, 900, 1200, 1500 and 1800 K.

Burn-up calculations can be executed as a part or complete application. However, memory usage might be a limiting factor for large systems when defining the number of depletion zones. There is no need for an additional user effort for selection of fission products and actinide daughter nuclides and the irradiation history is defined in units of time and burn-up. Reaction rates are normalized to total power, specific power density, flux or fission rate.

It can produce homogenized multi-group constants for deterministic reactor core simulators, which is important for the current work. The standard output contains:

- Effective and infinite multiplication factors calculated using different methods
- Homogenized few-group cross sections
- Group-transfer probabilities and scattering matrices
- Diffusion coefficients calculated using two fundamentally different methods
- P_n scattering cross sections up to order 5
- Assembly pin-power distributions

Homogenization can be done for multiple universes where group constants for several assemblies are produced within a single run. The user defines the number and borders of few-energy groups for the group constant generation.

The results for burn-up calculation are given as material-wise and total values, and consist of isotopic compositions, transmutation cross sections, activities and decay heat data.

All numerical output is written in MATLAB m-format files for simplification of post-processing of several calculation cases. A geometry plotter feature and a reaction rate plotter are also available for the code.

Serpent has been widely validated in light water reactor lattice calculations. Results for effective multiplication factors and homogenized few-group cross sections are within the statistical accuracy from reference MCNP results when the same ACE libraries are used.

Comparison to a similar calculation suggests that Serpent may run 80 times faster than codes like MCNP. The reason of the difference is not from the efficiency of the code but rather from the fact of large reaction rate tallies of MCNP. The important point is that Serpent can run full-scale assembly burn-up calculations similar to deterministic transport codes, and overall calculation time is counted in hours or days, rather than weeks or months. [4]

Monte Carlo (MC) methods are stochastic techniques, meaning they are based on the use of random numbers and probability statistics to investigate problems. You can find MC methods used in everything from economics to nuclear physics to regulating the flow of traffic. Of course the way they are applied varies widely from field to field, and there are dozens of subsets of MC even within chemistry. But, strictly speaking, to call something a "Monte Carlo" experiment, all you need to do is use random numbers to examine some problem.

The use of MC methods to model physical problems allows us to examine more complex systems than we otherwise can. Solving equations which describe the interactions between two atoms is fairly simple; solving the same equations for hundreds or thousands of atoms is impossible. With MC methods, a large system can be sampled in a number of random configurations, and that data can be used to describe the system as a whole.

The Monte Carlo method provides approximate solutions to a variety of mathematical problems by performing statistical sampling experiments on a computer. The method applies to problems with no probabilistic content as well as to those with inherent probabilistic structure. Among all numerical methods that rely on N -point evaluations in M -dimensional space to produce an approximate solution, the Monte Carlo method has absolute error of estimate that decreases as N superscript $-1/2$ whereas, in the absence of exploitable special structure all others have errors that decrease as N superscript $-1/M$ at best.

3.3 PARCS

PARCS is a three-dimensional reactor core simulator which solves the steady-state and time-dependent, multi-group neutron diffusion and SP3 transport equations in orthogonal and non-orthogonal geometries. PARCS is coupled directly to the thermal-hydraulics system code TRACE from which flow field information and temperature are provided to PARCS during transient calculations.

The major calculation features in PARCS are eigenvalue calculations, transient (kinetics) calculations, and adjoint calculations for commercial LWRs. Three-dimensional calculation model is the primary use of PARCS for the realistic representation of the physical reactors. However, for faster simulations for a group of transients, one-dimensional modeling is available when dominant variation of the flux is in the axial direction.

The input system in PARCS is card name based while default input parameters are maximized and the amount of the input data is minimized. For the continuation of the transient calculations, a restart feature is available, where the calculation restarts from the point that restart file was written. Various edit options are available in PARCS, also an on-line graphics feature that provides a quick and versatile visualization of the various physical phenomena occurring during transient calculation.

Accomplishing different tasks with high efficiency is established by incorporating numerous sophisticated spatial kinetics methods into PARCS. For spatial discretization, a variety of solution kernels are available to include the most popular LWR two group nodal methods, the Analytic Nodal Method (ANM) and the Nodal Expansion Method (NEM).

The usage of the advanced numerical solution methods minimizes the computational burden. The eigenvalue calculation to establish the initial steady-state is performed using the Wielandt eigenvalue shift method. When using the two nodal group methods, a pin power reconstruction method is available in which predefined heterogeneous power form functions are combined with a homogeneous intranodal flux distribution.

Two modes are available for one-dimensional calculations: normal one-dimensional and quasi-static one-dimensional. The normal one-dimensional mode uses a one-dimensional geometry and precollapsed one-dimensional group constants, while the quasi-static one-dimensional keeps the three-dimensional geometry and cross sections but performs the neutronic calculation in the one-dimensional mode using group constants which are collapsed during the transient. To preserve the three-dimensional planar averaged currents in the subsequent one-dimensional calculations, current conservation factors are employed in one-dimensional calculations during one-dimensional group constant generation. PARCS is also capable of performing core depletion analysis by introducing burn-up dependent macroscopic cross sections.

The calculation features of PARCS are as follows;

- Eigenvalue calculation
- Transient calculation
- Xenon/Samarium calculation
- Decay heat calculation
- Pin power calculation
- Adjoint calculation

There are many PARCS calculation methods, which are directly related to execution control, which users can choose the proper options suiting best for their needs. The method used for this thesis is 2 group nodal methods. The spatial solution of the neutron flux in the reactor is determined in PARCS using well-established numerical methods. Nodal methods are the primary means used in PARCS to obtain higher order solutions to the neutron diffusion equation solving the two-node problem.

The ANM is regarded as one of the more accurate techniques for solving the neutron diffusion equation. The only approximation required is that used for the shape of the transverse leakage sources which appear in the one-dimensional, transverse integrated flux equations. Although the analytic nature of this method is responsible for its remarkable accuracy, it has thus far lead to algebraically complicated expressions for the nodal coupling relations which, for all practical purposes, appears to restrict the ANM to only two energy group problems. This apparent limitation is

not due to the method itself, but arises as a result of the original approach taken for the evaluation of the nodal coupling relations. The preparation of these coupling coefficients relies on the evaluation of trigonometric functions of G by G matrices. These expressions become increasingly complicated as the number of energy groups increases.

The first polynomial method was NEM. In fact, although some variations and improvements have been considered, the NEM ideology still dominates the polynomial class of nodal methods. In this lowest order form, NEM considers a quadratic expansion of the transverse averaged flux (i.e. $\phi_j(x)$ and $\phi_j(y)$) on each cell. The expansion coefficients are determined by applying Fick's law in combination with discrete nodal balance equation and continuity of normal current. Considerable effort has been made to utilize higher order polynomial expansion within NEM. The difficulty this creates is centered around the evaluation of the higher order expansion coefficients. In particular, the weighted residual procedure that is typically used relies on transverse-integrated and as a result an approximation of the transverse normal currents (i.e. transverse leakage) is also required.

ANM in PARCS has been used frequently within the LWR industry to solve the two-group diffusion equation. When there is no net leakage out of a node and the ANM matrix becomes singular, the problem is called as critical node problem and methods were added to PARCS to address this problem. The second nodal method, NEM was added which does not have this potential problem, but is less accurate for certain types of problems. Replacement of ANM two-node problem by a NEM two-node problem for the near critical nodes is available with a hybrid ANM-NEM method. The user specifies a tolerance on the difference in the node k_{inf} and k_{eff} which is used to switch between the ANM and NEM kernels. NEM is also available in a multi-group form for both Cartesian and hexagonal geometries. [5]

4. DESCRIPTION OF MINI CORE PROBLEMS

The major work done on this thesis is developing a method of ADF generation for fuel-reflector interface without explicit knowledge of heterogeneous interface conditions and verifying the developed technique by Serpent and PARCS. The purpose is to achieve correct core k_{eff} and flux ratios (the ratio of average fast flux to average thermal flux in the assembly) for each assembly.

4.1 Main Properties of The Core Assemblies

Each assembly consists of 100 pins, which are placed in 10x10 lattice. The pin lattices are square lattices as well as the same is for the assemblies. There are two types of assemblies: fuel assembly and reflector assembly. The fuel assembly consists of the same type and enrichment (3.8% U-235) of fuel pins. The fuel pin has a fuel pellet which has a diameter of 0.848 cm, and the diameter of the inner clad is 0.863 cm and the outer clad is 0.984 cm (see Fig. 4.1). The gap between the fuel pellet and the inner clad is filled with Helium. The pitch size is 1.8 cm for both fuel and reflector assemblies and the assembly size is 18.0 cm. The reflector assembly is filled with water.

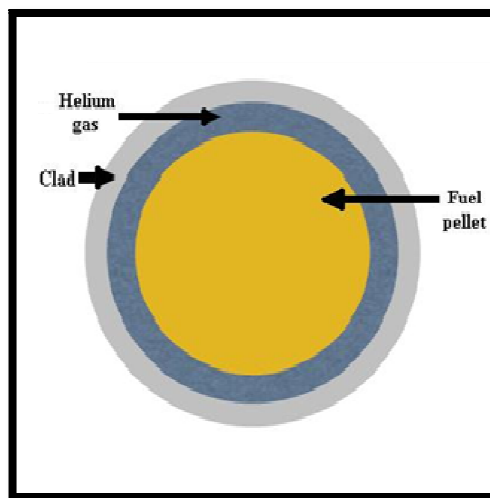


Figure 4.1 : The cross section area of the fuel pin.

4.2 Application of The Verification and The Homogenization

The verification process starts by homogenizing the given core design. First, a Serpent model with the geometry and material properties of the core is created. The model is executed to generate two-group constants and diffusion parameters that are generated for each assembly separately, so that each assembly is homogenized explicitly. For the same core, another Serpent execution is done to generate two-group constants over the whole core to be able to calculate k_{eff} . k_{eff} is the eigenvalue of the neutron balance equation. The balance is between losses and gains of neutrons. The losses are the absorption and the out-scattering neutrons. And the gains are the fission and the in-scattering neutrons. The two-group eigenvalue equation is written as follows;

$$k \begin{bmatrix} \Phi_1 \\ \Phi_2 \end{bmatrix} = [A + S_{out} - S_{in}]^{-1} [F] \begin{bmatrix} \Phi_1 \\ \Phi_2 \end{bmatrix} \quad (4.1)$$

where

$A = \begin{bmatrix} \Sigma_{a1} & 0 \\ 0 & \Sigma_{a2} \end{bmatrix}$ is the absorption cross section matrix

$S_{in} = \begin{bmatrix} 0 & \Sigma_{1 \leftarrow 2} \\ \Sigma_{2 \leftarrow 1} & 0 \end{bmatrix}$ is the in-scattering cross section matrix

$S_{out} = \begin{bmatrix} \Sigma_{2 \leftarrow 1} & 0 \\ 0 & \Sigma_{1 \leftarrow 2} \end{bmatrix}$ is the out-scattering cross section matrix,

$F = \begin{bmatrix} \chi_1 \nu \Sigma_{f1} & \chi_1 \nu \Sigma_{f2} \\ \chi_2 \nu \Sigma_{f1} & \chi_2 \nu \Sigma_{f2} \end{bmatrix}$ is the fission cross section matrix

k is the eigenvalue of the solution which gives us the k_{eff} .

As Serpent is the first step of the process where the assembly homogenization takes place, PARCS is the second step of the process where the results are verified. For the same core, PARCS model is created where geometry, two-group constants and discontinuity factors are defined. After the execution of the model, output of PARCS gives the k_{eff} value and fast and thermal fluxes of each assembly. Finally, results were compared to verify the error between PARCS and Serpent.

4.2.1 Generation of the assembly discontinuity factors

The basic parameters, which are converted from one code to the other, are few-group constants and assembly discontinuity factors. Serpent is capable to generate the correct few-group constants for single and multi-assembly problem but it is not capable of generating correct ADFs for multi-assembly problem. The ADFs were generated off-line for a set of 2x2 cores (see Fig. 4.4, Fig. 4.5 and Fig. 4.6) in a typical fuel-reflector configuration.

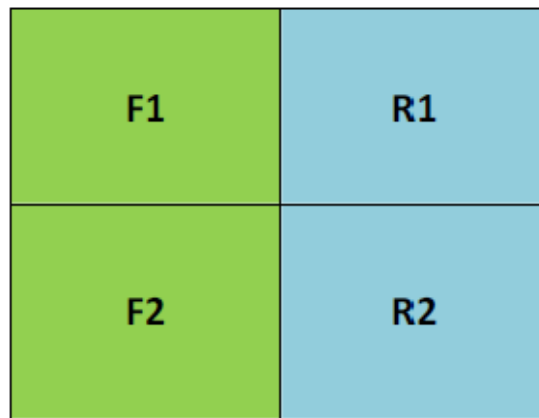


Figure 4.2 : Geometry of combination-1.

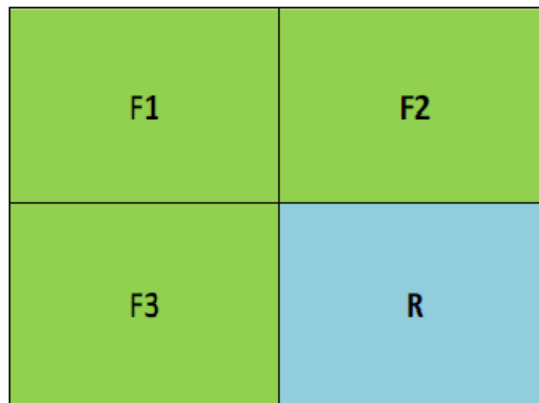


Figure 4.3 : Geometry of combination-2.

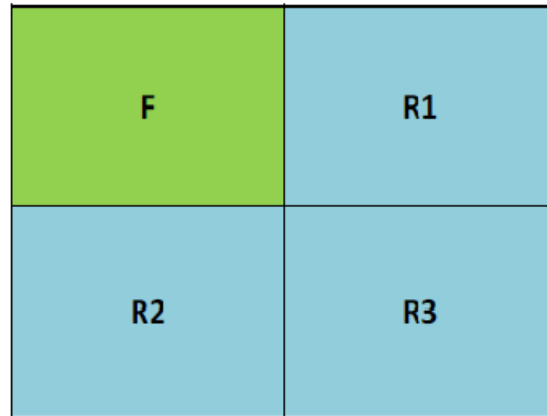


Figure 4.4 : Geometry of combination-3.

The two-group constants for each assembly were generated by Serpent and then introduced into the cross section card of PARCS. To be able to find the ADFs that give the best k_{eff} and best flux ratio results, a set of ADFs was generated and tested with a value region of 0.01 to 1.0.

The k_{eff} and flux ratio results were compared with the reference and the optimum ADF was found. The final choice of ADFs and the results for each combination are seen at the Table from 4.1 to 4.6 (detailed plots of the results are given in the Appendix A.1, A.2 and A.3).

Table 4.1: ADFs for fuel and reflector assemblies for combination-1

Composition	ADF fast group	ADF thermal group
F ₁ , F ₂	1.0	1.0
R ₁ , R ₂	0.54	0.55

Table 4.2: Comparison of solutions of combination-1

	k_{eff}	Assembly F ₁ Flux Ratio	Assembly F ₂ Flux Ratio	Assembly R ₁ Flux Ratio	Assembly R ₂ Flux Ratio
Reference solution	1.26721	2.325	2.325	0.375	0.376
UDF solution	+1.8%	-0.4%	-0.4%	+4.9%	+4.9%
ADF solution	0.0%	-0.1%	-0.1%	-0.6%	-0.6%

Table 4.3: ADFs for fuel and reflector assemblies for combination-2

Composition	ADF fast group	ADF thermal group
F ₁ , F ₂ , F ₃	1.0	1.0
R	0.62	0.57

Table 4.4: Comparison of solutions of combination-2

	k_{eff}	Assembly F ₁ Flux Ratio	Assembly F ₂ Flux Ratio	Assembly F ₃ Flux Ratio	Assembly R Flux Ratio
Reference solution	1.34083	2.356	2.283	0.282	0.401
UDF solution	+0.9%	+0.3%	+0.1%	+0.1%	+5.0%
ADF solution	0.0%	+0.4%	+0.3%	+0.3%	-1.9%

Table 4.5: ADFs for fuel and reflector assemblies for combination-3

Composition	ADF fast group	ADF thermal group
F	1.0	1.0
R ₁ , R ₂ , R ₃	0.40	0.56

Table 4.6: Comparison of solutions of combination-3

	k_{eff}	Assembly F Flux Ratio	Assembly R ₁ Flux Ratio	Assembly R ₂ Flux Ratio	Assembly R ₃ Flux Ratio
Reference solution	1.12928	2.336	0.381	0.381	0.293
UDF solution	+4.1%	-0.7%	+5.1%	+5.0%	-4.5%
ADF solution	0.0%	-0.7%	+1.0%	+0.9%	-5.7%

Reference solution is the result from Serpent, UDF solution is the results without ADFs and ADF solution is the results with ADFs. The results prove that the ADFs make a remarkable improvement in k_{eff} and flux ratios prediction.

In addition, it is seen that the thermal ADF in each three case is very close to each other. As the thermal group ADF is more important than the fast group ADF, in the mini core problems it is also possible to use average ADFs (aADFs) which will be the average of the three cases that ADFs were generated.

5. PRESENTATION AND DISCUSSION OF RESULTS

In Chapter 4 it was explained how the ADFs were calculated. Once the ADFs were determined in Chapter 4, they were tested on 14 different mini cores consisting of fuel and reflector assemblies in 5x5 configuration (the configuration of the geometries of each core is shown in the Appendix B.1). The results with and without ADFs are shown in Table from 5.1 to 5.14.

Table 5.1: Comparison of solutions of mini core-1

	k_{eff}	Assembly R ₁ Flux Ratio	Assembly F ₁ Flux Ratio
Reference solution	1.39765	0.376	2.335
UDF solution	+0.42%	+4.5%	+0.4%
ADF solution	+0.33%	-0.9%	+0.4%
aADF solution	+0.32%	-0.2%	+0.3%

Table 5.2: Comparison of solutions of mini core-2

	k_{eff}	Assembly R ₁ Flux Ratio	Assembly F ₂₄ Flux Ratio
Reference solution	1.42596	0.401	2.323
UDF solution	-0.10%	-2.0%	+3.8%
ADF solution	-0.12%	-7.6%	+3.7%
aADF solution	-0.13%	-6.9%	+3.8%

Table 5.3: Comparison of solutions of mini core-3

	k_{eff}	Assembly R ₁ Flux Ratio	Assembly F ₂₁ Flux Ratio
Reference solution	1.41708	0.410	2.332
UDF solution	-0.33%	+5.6%	+10.1%
ADF solution	-0.39%	-1.4%	+10.1%
aADF solution	-0.41%	-0.3%	+10.1%

Table 5.4: Comparison of solutions of mini core-4

	k_{eff}	Assembly R ₉ Flux Ratio	Assembly F ₁₆ Flux Ratio
Reference solution	1.39508	0.408	2.338
UDF solution	+0.22%	+4.9%	+3.7%
ADF solution	+0.04%	-2.0%	+3.8%
aADF solution	+0.01%	-0.9%	+3.8%

Table 5.5: Comparison of solutions of mini core-5

	k_{eff}	Assembly R ₁ Flux Ratio	Assembly F ₅ Flux Ratio
Reference solution	1.26674	0.379	2.326
UDF solution	+1.91%	+4.4%	-0.5%
ADF solution	+0.03%	-1.2%	-0.2%
aADF solution	+0.11%	-0.6%	-0.4%

Table 5.6: Comparison of solutions of mini core-6

	k_{eff}	Assembly R ₁₃ Flux Ratio	Assembly F ₃ Flux Ratio
Reference solution	1.37384	0.377	2.344
UDF solution	+0.68%	+4.5%	+0.1%
ADF solution	+0.37%	-1.1%	+0.1%
aADF solution	+0.34%	-0.5%	+0.1%

Table 5.7: Comparison of solutions of mini core-7

	k_{eff}	Assembly R ₇ Flux Ratio	Assembly F ₁ Flux Ratio
Reference solution	1.40274	0.377	2.330
UDF solution	+0.35%	+4.3%	+0.3%
ADF solution	+0.25%	-1.3%	+0.3%
aADF solution	+0.24%	-0.7%	+0.3%

Table 5.8: Comparison of solutions of mini core-8

	k_{eff}	Assembly R ₅ Flux Ratio	Assembly F ₁₇ Flux Ratio
Reference solution	1.41457	0.373	2.330
UDF solution	+0.22%	+4.5%	+0.4%
ADF solution	+0.17%	-1.0%	+0.4%
aADF solution	+0.16%	-0.4%	+0.4%

Table 5.9: Comparison of solutions of mini core-9

	k_{eff}	Assembly R ₃ Flux Ratio	Assembly F ₅ Flux Ratio
Reference solution	1.25739	0.378	2.396
UDF solution	+1.75%	+6.0%	+4.0%
ADF solution	+0.29%	+0.6%	+4.2%
aADF solution	+0.34%	+1.4%	+4.1%

Table 5.10: Comparison of solutions of mini core-10

	k_{eff}	Assembly R ₂ Flux Ratio	Assembly F ₇ Flux Ratio
Reference solution	1.29401	0.408	2.379
UDF solution	+1.06%	+6.3%	+5.8%
ADF solution	-0.16%	+0.2%	+5.9%
aADF solution	-0.07%	0.0%	+5.9%

Table 5.11: Comparison of solutions of mini core-11

	k_{eff}	Assembly R ₁ Flux Ratio	Assembly F ₁₁ Flux Ratio
Reference solution	1.38662	0.400	2.337
UDF solution	+0.28%	+5.9%	+3.4%
ADF solution	-0.05%	-1.1%	+3.5%
aADF solution	-0.14%	-0.1%	+3.5%

Table 5.12: Comparison of solutions of mini core-12

	k_{eff}	Assembly R ₁ Flux Ratio	Assembly F ₁ Flux Ratio
Reference solution	1.41511	0.432	2.329
UDF solution	+0.14%	+5.0%	+0.5%
ADF solution	-0.01%	-3.1%	+0.5%
aADF solution	-0.05%	-2.0%	+0.5%

Table 5.13: Comparison of solutions of mini core-13

	k_{eff}	Assembly R ₅ Flux Ratio	Assembly F ₂₀ Flux Ratio
Reference solution	1.37307	0.420	2.347
UDF solution	+0.62%	+4.9%	+0.3%
ADF solution	+0.21%	-2.7%	+0.3%
aADF solution	+0.1%	-1.6%	+0.4%

Table 5.14: Comparison of solutions of mini core-14

	k_{eff}	Assembly R ₄ Flux Ratio	Assembly F ₅ Flux Ratio
Reference solution	1.32844	0.371	2.362
UDF solution	+1.09%	+5.1%	+0.3%
ADF solution	+0.19%	-0.8%	+0.4%
aADF solution	-0.04%	-0.5%	+0.4%

In general, the error in the results reduces remarkably with the use of ADFs. We can see that the generated few-group constants by Serpent are reliable, because the reduction error occurs with the use of correctly designed ADFs.

The three different discontinuity factor solutions (UDF, ADF and aADF) gave the same flux ratio results for the fuel assemblies because the value of the discontinuity factors in each solution is always 1.0 for fuel assemblies. However, the ADF and aADF solutions for the reflector assemblies, which have at least one interface with the fuel assemblies, had a remarkable improvement in the flux ratio results.

The ADF and aADF solutions always gave very good k_{eff} results. However, the UDF solution gave inconsistent k_{eff} results. The inconsistency is because of the number of the fuel assemblies in each configuration. The configurations which had a high number of fuel assemblies gave closer k_{eff} results to the reference solution, because there were fewer reflector assemblies, where the flux distribution was not correct. However, when the number of reflector assemblies increased, the UDF solution gave bad k_{eff} results.

The thermal flux group is more important than the fast flux group in light water reactors. The value of aADF thermal discontinuity factor is very similar to the values of ADF thermal discontinuity factor. Therefore, aADF solution gave similar results as ADF solution.

6. CONCLUSION

The major purpose of this research was to verify the assembly homogenization capability of Serpent. Since assembly power distribution is very important for commercial reactors, the study is important for the application of Serpent as a tool for cross section homogenization. The conclusion for few-group constant generation is that Serpent is capable to generate few-group constants that can be used in a deterministic reactor code. However, generation of ADFs for fuel-reflector interface has to be done off-line by a separate method, as presented in this thesis. The effect of ADFs is significant and cannot be neglected. With correct ADFs, the homogeneous nodal solution errors were acceptable for every mini core.

As Serpent is much faster than MCNP and being highly efficient, it is recommended that it is developed to generate correct ADFs for multi-assembly models.

The current study was done in two-dimensional geometry and with two type assemblies, so further studies should be done for three-dimensional geometries and multi type assemblies.

REFERENCES

- [1] **Stacey W. M.**, 2001, Nuclear Reactor Physics, John Wiley & Sons, INC., U.S.A.
- [2] **Smith, K. S.**, 1986: Assembly Homogenization Techniques For Light Water Reactor Analysis. *Progress in Nuclear Energy*, Vol.17, No. 3, pp. 303-335, Pergamon Journals Ltd., Great Britain.
- [3] **Koebke, K.**, 1978. A New Approach To Homogenization and Group Condensation. In: *IAEA Technical Committee Meeting on Homogenization Methods in Reactor Physics*, Lugano, Switzerland, 13-15 November, IAEA-TECDOC 231.
- [4] **Lappänen, J.**, 2010. PSG2 / Serpent – a Continuous-energy Monte Carlo Reactor Physics Burn-up Calculation Code. VTT Technical Research Centre of Finland.
- [5] **Downar, T., Xu, Y., Seker, V. And Carlson, D.**, 2007. PARCS v2.7 U.S. NRC Core Neutronics Simulator. School of Nuclear Engineering, Purdue University, W. Lafayette, Indiana, U.S.A. and RES / U.S. NRC, Rockville, Md, U.S.A..

APPENDICES

APPENDIX A.1: Surface plots of errors of designing ADFs for combination-1

APPENDIX A.2: Surface plots of errors of designing ADFs for combination-2

APPENDIX A.3: Surface plots of errors of designing ADFs for combination-3

APPENDIX B.1: Configuration of the geometry for each core

APPENDIX A.1

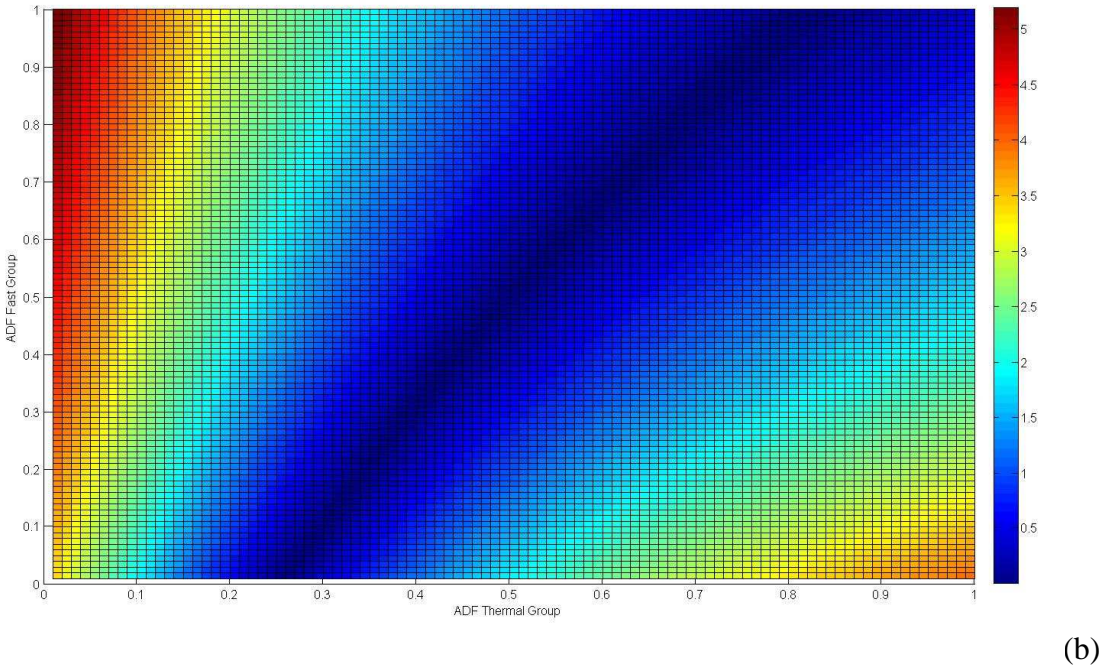
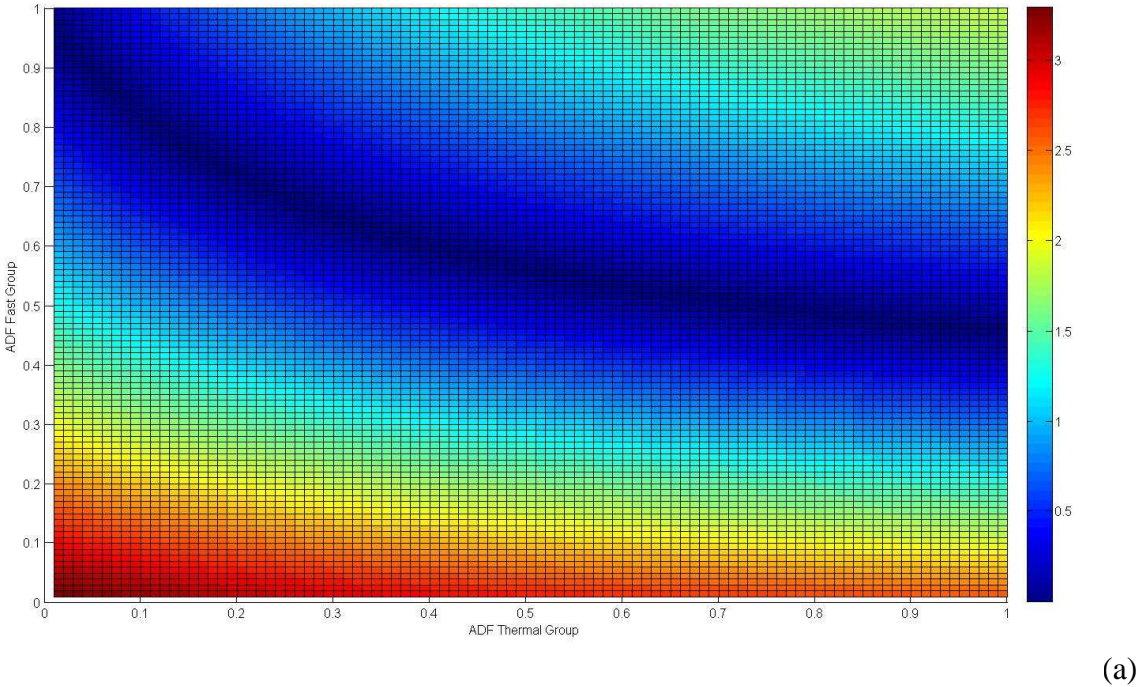


Figure A.1 : Surface plots of errors of designing ADFs for combination-1:
(a)K-effective. (b)Fuel flux ratio. (c)Reflector flux ratio.

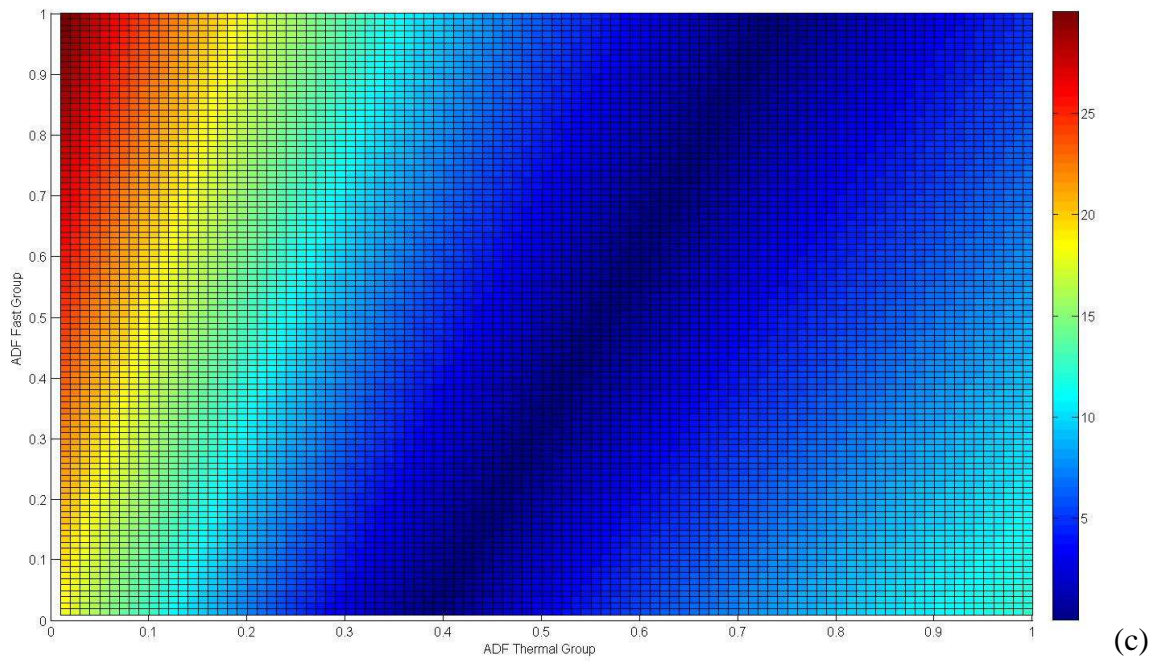


Figure A.1(contd.) : Surface plots of errors of designing ADFs for combination-1:
 (a)K-effective. (b)Fuel flux ratio. (c)Reflector flux ratio.

APPENDIX A.2

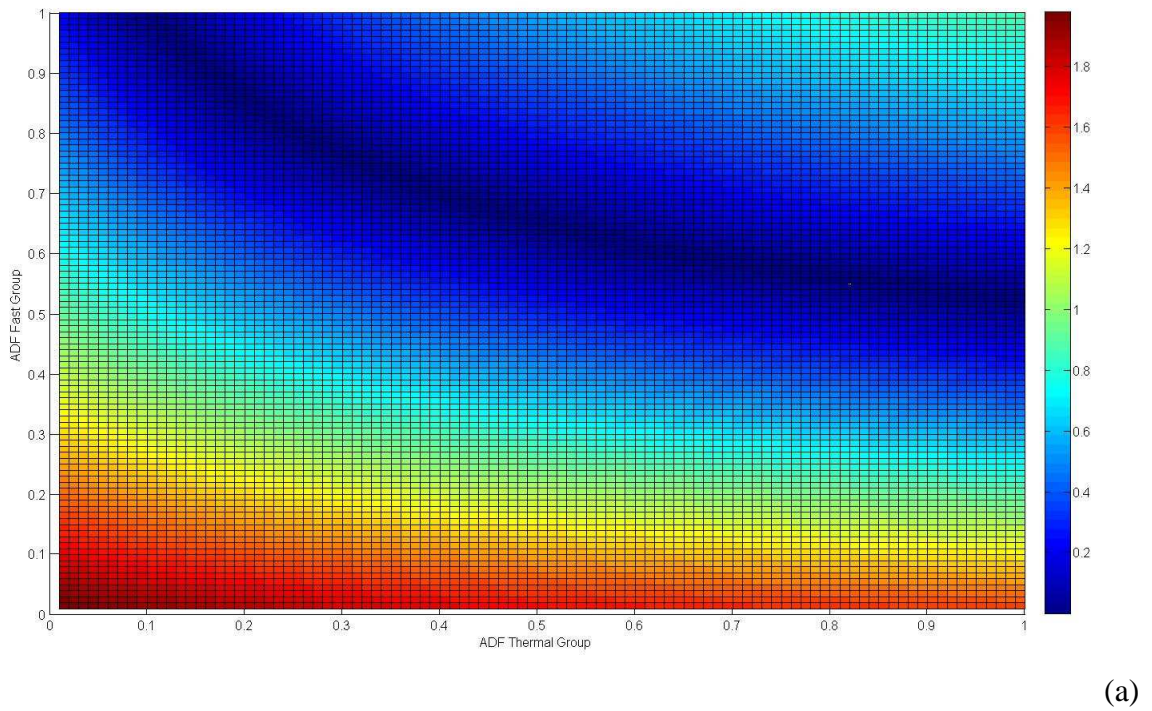


Figure A.2 : Surface plots of errors of designing ADFs for combination-2:
 (a)K-effective. (b)Fuel flux ratio. (c)Reflector flux ratio.

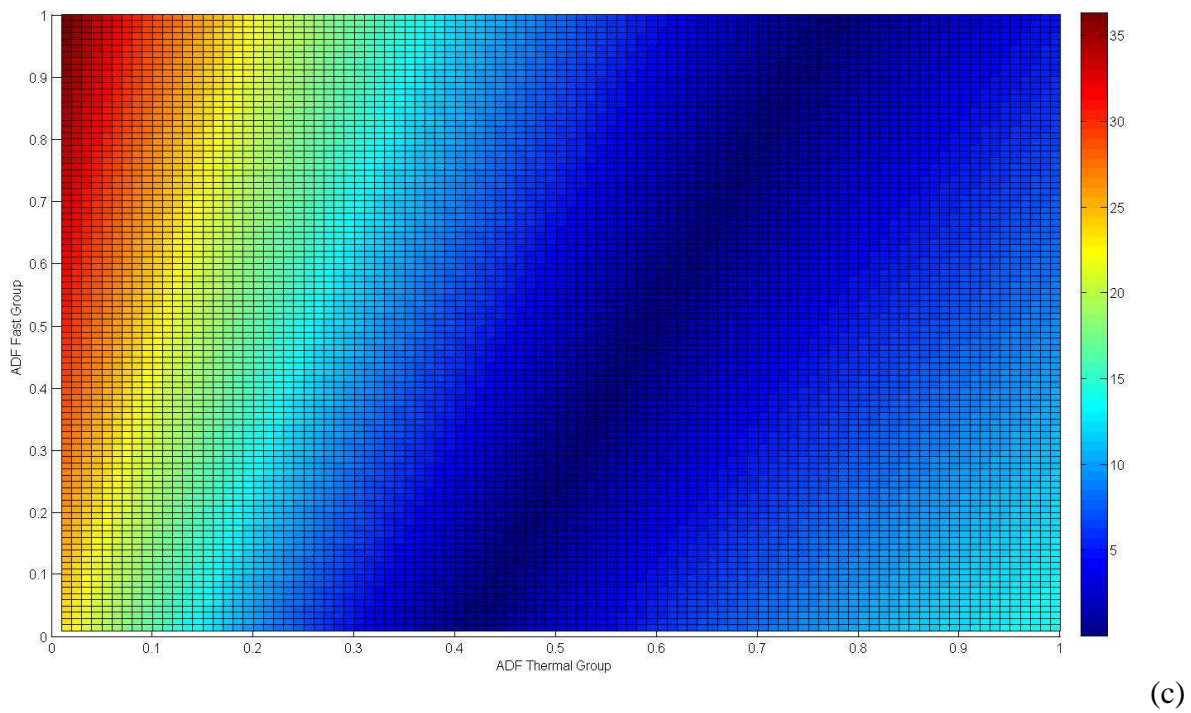
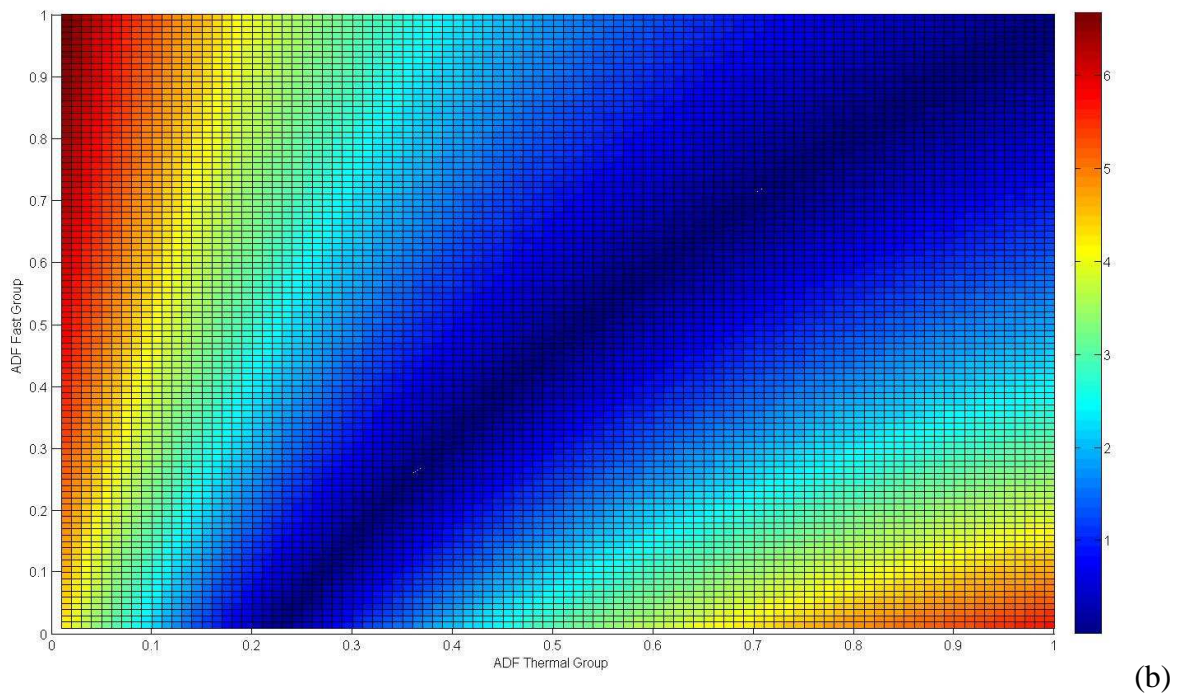


Figure A.2(contd.) : Surface plots of errors of designing ADFs for combination-2:
 (a)K-effective. (b)Fuel flux ratio. (c)Reflector flux ratio.

APPENDIX A.3

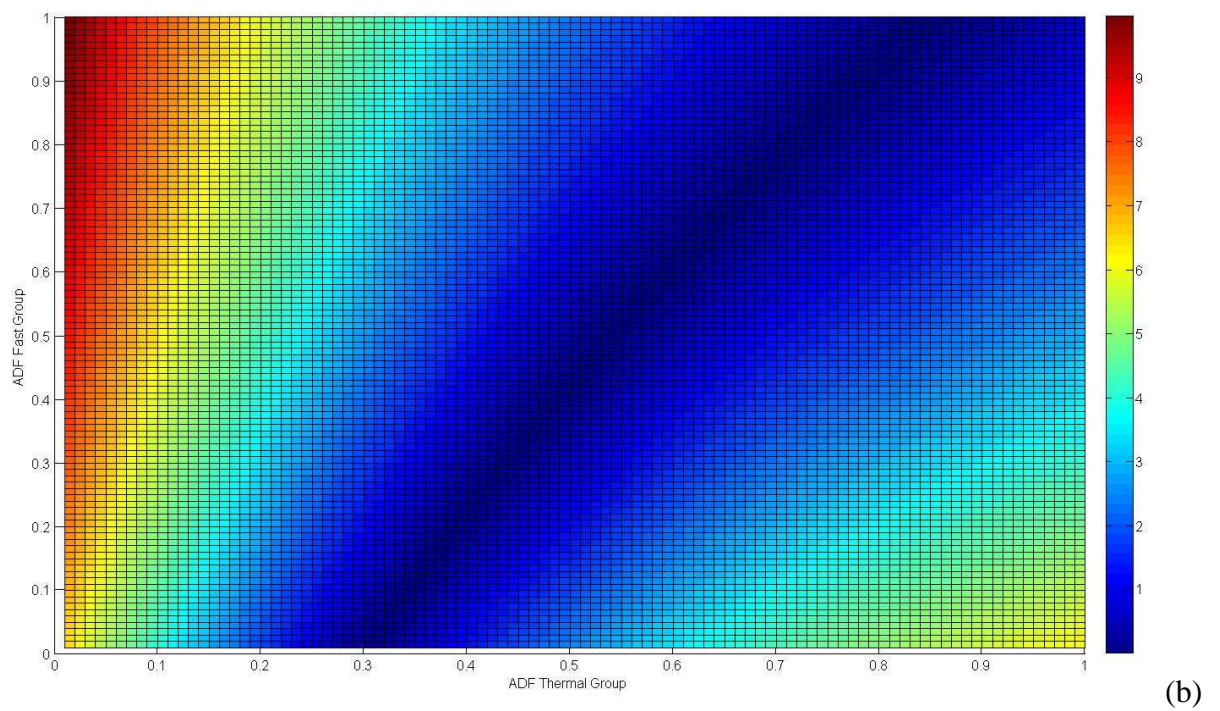
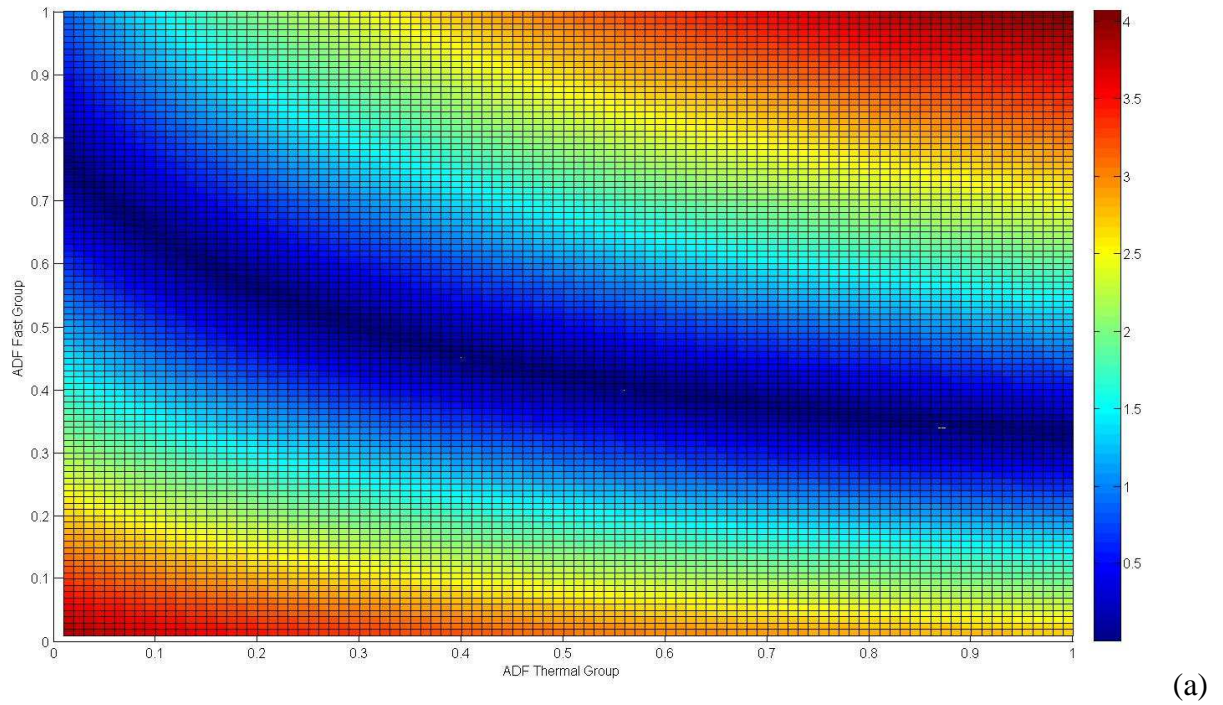


Figure A.3 : Surface plots of errors of designing ADFs for combination-3:
(a)K-effective. (b)Fuel flux ratio. (c)Reflector flux ratio.

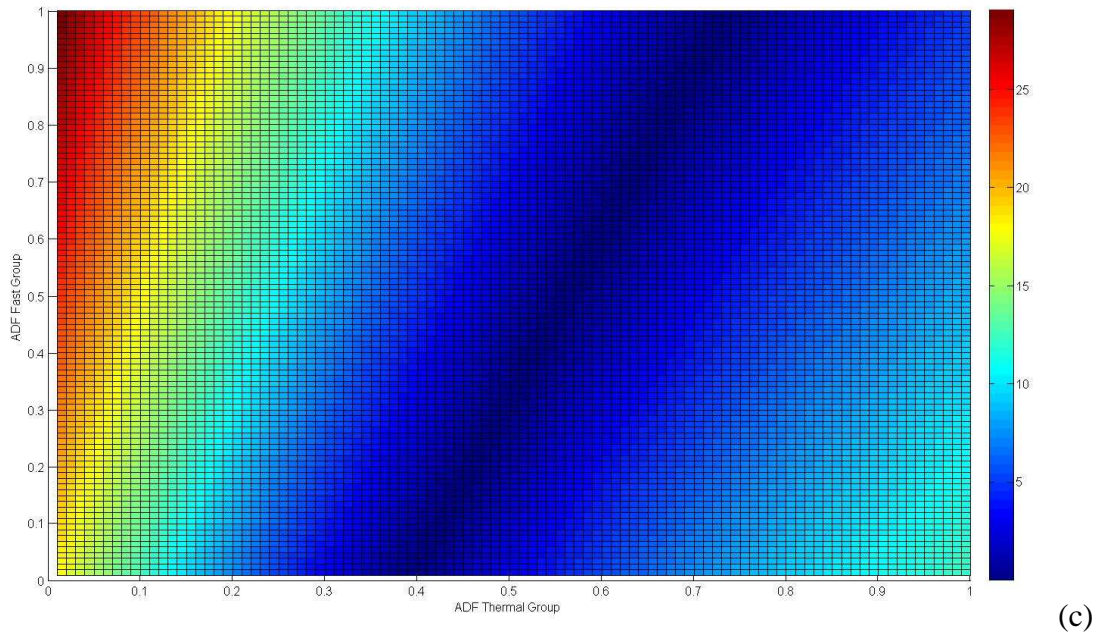


Figure A.3(contd.) : Surface plots of errors of designing ADFs for combination-3:
(a)K-effective. (b)Fuel flux ratio. (c)Reflector flux ratio.

APPENDIX B.1

F ₁	F ₂	F ₃	F ₄	R ₁
F ₅	F ₆	F ₇	F ₈	R ₂
F ₉	F ₁₀	F ₁₁	F ₁₂	R ₃
F ₁₃	F ₁₄	F ₁₅	F ₁₆	R ₄
R ₅	R ₆	R ₇	R ₈	R ₉

R ₁	F ₁	F ₂	F ₃	F ₄
F ₅	F ₆	F ₇	F ₈	F ₉
F ₁₀	F ₁₁	F ₁₂	F ₁₃	F ₁₄
F ₁₅	F ₁₆	F ₁₇	F ₁₈	F ₁₉
F ₂₀	F ₂₁	F ₂₂	F ₂₃	F ₂₄

(a)

(b)

R ₁	R ₂	F ₁	F ₂	F ₃
R ₃	R ₄	F ₄	F ₅	F ₆
F ₇	F ₈	F ₉	F ₁₀	F ₁₁
F ₁₂	F ₁₃	F ₁₄	F ₁₅	F ₁₆
F ₁₇	F ₁₈	F ₁₉	F ₂₀	F ₂₁

R ₁	R ₂	R ₃	F ₁	F ₂
R ₄	R ₅	R ₆	F ₃	F ₄
R ₇	R ₈	R ₉	F ₅	F ₆
F ₇	F ₈	F ₉	F ₁₀	F ₁₁
F ₁₂	F ₁₃	F ₁₄	F ₁₅	F ₁₆

(c)

(d)

F ₁	R ₁	R ₂	R ₃	R ₄
F ₂	R ₅	R ₆	R ₇	R ₈
F ₃	R ₉	R ₁₀	R ₁₁	R ₁₂
F ₄	R ₁₃	R ₁₄	R ₁₅	R ₁₆
F ₅	R ₁₇	R ₁₈	R ₁₉	R ₂₀

F ₁	F ₂	R ₁	R ₂	R ₃
F ₃	F ₄	R ₄	R ₅	R ₆
F ₅	F ₆	R ₇	R ₈	R ₉
F ₇	F ₈	R ₁₀	R ₁₁	R ₁₂
F ₉	F ₁₀	R ₁₃	R ₁₄	R ₁₅

(e)

(f)

Figure B.1 : Configuration of the geometry for each core: (a)mini core-1. (b)mini core-2. (c)mini core-3. (d)mini core-4. (e)mini core-5. (f)mini core-6. (g)mini core-7. (h)mini core-8. (i)mini core-9. (j)mini core-10. (k)mini core-11. (l)mini core-12. (m)mini core-13. (n)mini core-14.

F ₁	F ₂	F ₃	R ₁	R ₂
F ₄	F ₅	F ₆	R ₃	R ₄
F ₇	F ₈	F ₉	R ₅	R ₆
F ₁₀	F ₁₁	F ₁₂	R ₇	R ₈
F ₁₃	F ₁₄	F ₁₅	R ₉	R ₁₀

(g)

F ₁	F ₂	F ₃	F ₄	R ₁
F ₅	F ₆	F ₇	F ₈	R ₂
F ₉	F ₁₀	F ₁₁	F ₁₂	R ₃
F ₁₃	F ₁₄	F ₁₅	F ₁₆	R ₄
F ₁₇	F ₁₈	F ₁₉	F ₂₀	R ₅

(h)

R ₁	R ₂	R ₃	R ₄	R ₅
R ₆	F ₁	F ₂	F ₃	R ₇
R ₈	F ₄	F ₅	F ₆	R ₉
R ₁₀	F ₇	F ₈	F ₉	R ₁₁
R ₁₂	R ₁₃	R ₁₄	R ₁₅	R ₁₆

(i)

R ₁	R ₂	F ₁	R ₃	R ₄
R ₅	F ₂	F ₃	F ₄	R ₆
F ₅	F ₆	F ₇	F ₈	F ₉
R ₇	F ₁₀	F ₁₁	F ₁₂	R ₈
R ₉	R ₁₀	F ₁₃	R ₁₁	R ₁₂

(j)

R ₁	F ₁	F ₂	F ₃	R ₂
F ₄	F ₅	F ₆	F ₇	F ₈
F ₉	F ₁₀	F ₁₁	F ₁₂	F ₁₃
F ₁₄	F ₁₅	F ₁₆	F ₁₇	F ₁₈
R ₃	F ₁₉	F ₂₀	F ₂₁	R ₄

(k)

F ₁	F ₂	F ₃	F ₄	F ₅
F ₆	F ₇	F ₈	F ₉	F ₁₀
F ₁₁	F ₁₂	R ₁	F ₁₃	F ₁₄
F ₁₅	F ₁₆	F ₁₇	F ₁₈	F ₁₉
F ₂₀	F ₂₁	F ₂₂	F ₂₃	F ₂₄

(l)

Figure B.1(contd.) : Configuration of the geometry for each core: (a)mini core-1. (b)mini core-2. (c)mini core-3. (d)mini core-4. (e)mini core-5. (f)mini core-6. (g)mini core-7. (h)mini core-8. (i)mini core-9. (j)mini core-10. (k)mini core-11. (l)mini core-12. (m)mini core-13. (n)mini core-14.

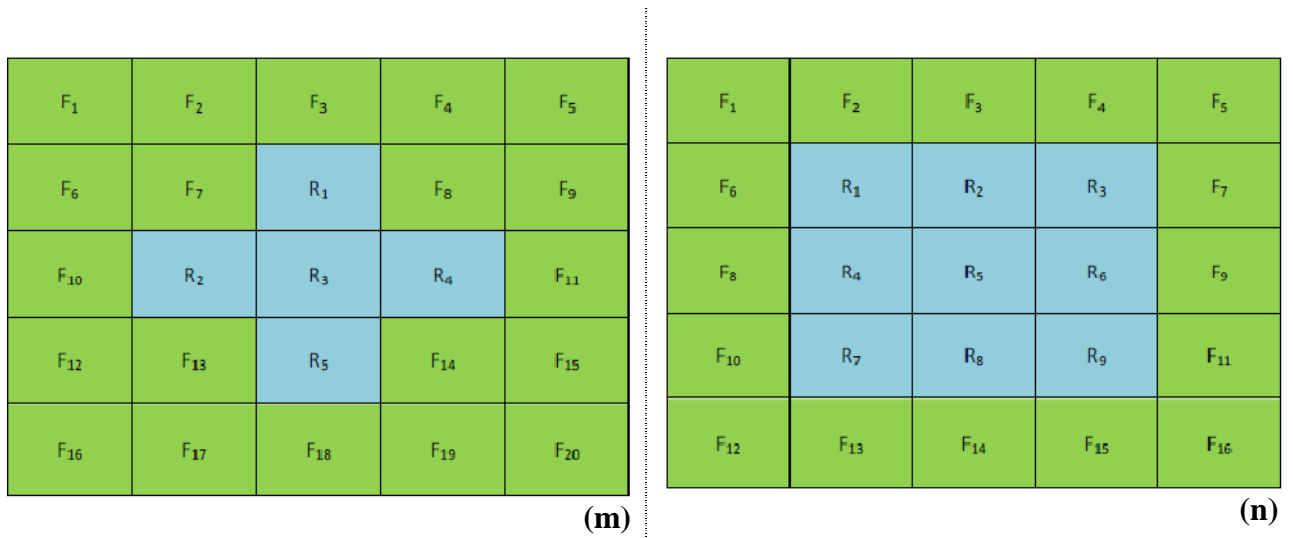


Figure B.1(contd.) : Configuration of the geometry for each core: (a)mini core-1. (b)mini core-2. (c)mini core-3. (d)mini core-4. (e)mini core-5. (f)mini core-6. (g)mini core-7. (h)mini core-8. (i)mini core-9. (j)mini core-10. (k)mini core-11. (l)mini core-12. (m)mini core-13. (n)mini core-14.

CURRICULUM VITA



Candidate's full name: Aziz Bora Pekicten

Place and date of birth: Darmstadt, GERMANY, 5 March 1985

Permanent Address: Hamit Oskay Sok. 5/8, 34730 Gztepe/İST

Universities and Colleges attended: Yildiz Technical University
Istanbul Technical University
Royal Institute of Technology